BALLISTIC-ELECTRON-EMISSION MICROSCOPY: A Nanometer-scale Probe of Interfaces and Carrier Transport

L. D. Bell and W. J. Kaiser

Center for Space Microelectronics Technology
Jet Propulsion Laboratory
California Institute of Technology
Pasadena, CA 91109

to appear in ANNUAL REVIEWS OF MATERIALS SCIENCE

CONTENTS

INTRODUCTION

Electron transport through materials and across interfaces is a fundamental focus of solid-state physics. [1,2] The investigation of semiconductor interfaces is complicated by their inaccessibility to conventional surface-analytical probes. Electronic characterization of completed interfaces has relied heavily on traditional electrical probes, such as current-voltage or capacitance-voltage measurements, or on optical methods such as internal photoemission. [3,4]

Scanning tunneling microscopy [5] (STM) is an extremely versatile probe of surfaces which can be used for both spectroscopy and imaging. [6] This review discusses ballistic-electron-emission microscopy [7-9] (BEEM), which provides similar capabilities for the study of interfaces. The method utilizes STM in a three-electrode configuration and allows characterization of interface properties with nanometer spatial resolution and enables an energy spectroscopy of carrier transport,

BEEM employs an STM tip to inject ballistic electrons into a sample heterostructure, illustrated in Figure 1 for the case of a metal/semiconductor (M/S) Schottky barrier (SB) system. The metal base layer serves as a reference electrode, and the semiconductor functions as a collector of ballistic electron current. As a negative tip voltage is applied, electrons tunnel into the base. Since attenuation lengths in metals and semiconductors may be tens of nanometers, [10] many of these hot electrons may reach the interface before scattering. If the tunnel voltage is greater than the barrier height ($V > V_b$), some of these electrons cross the interface into the semiconductor conduction band, and a collector current is observed. By varying the voltage between tip and base, the energy distribution of the electrons is varied, and a spectroscopy of carrier transport maybe performed. The location of the threshold in the spectrum defines the interface barrier height. The magnitude of the current above threshold and the spectrum shape also yield important information on the details of transport.

The BEEM process maybe understood by using a simple theoretical model, the essence of which is the description of the phase space available for interface transport. Scattering of particles during transport and dynamical considerations such as quantum mechanical reflection (QMR) are not included in this initial description, The simplest case to consider is that of a smooth interface between two materials with matching lattice nets, which dictates conservation of the component of the electron wave vector k_t transverse to the interface normal.

The tunnel current from tip to sample, using a planar tunneling formalism, [11] is given by

$$I_t = 2ea\iiint \frac{d^3\mathbf{k}}{(2\pi)^3} D(E_x) v_x [f(E) - f(E + eV)]$$
$$\propto \int_0^\infty dE_x D(E_x) \int_0^\infty dE_t [f(E) - f(E + eV)] \quad 1.$$

where $E_x = \hbar^2 k_x^2 / 2m$, $E_t = \hbar^2 k_t^2 / 2m$, a is the effective tunneling area, $f(E)$ is the Fermi distribution function, and $v_x = \hbar k_x / m$. For simplicity, the tip and base are assumed to have free-electron mass m; the component of semiconductor effective mass parallel to the interface is m_t. A similar expression may be written for the collector current by considering the subset of tip states which may conserve k_t across the interface. For the case of a zone-centered conduction-band minimum (CBM) and $m_t < m$, these restrictions on tip states are

$$E_t \leq \frac{m_t}{m - m_t} [Ex - EF + e(V - Vi))] \quad 2.$$

and

$$E_x \geq E_F - e(V - V_b) \ , \quad 3.$$

where E_F is the Fermi energy of the tip. Taking the equalities as limits E_t^{max} and E_x^{min}, collector current can be written as

$$I_c \propto R \int_{E_x\ min}^\infty dE_x D(E_x) \int_0^{E_t^{max}} dE_t [f(E) - f(E + eV)] \quad 4.$$

R is a measure of attenuation due to scattering in the base layer, taken to be energy-independent for these energies, [12] and at the interface. When Equation (4) is evaluated, the leading-order term is proportional to $(V - V_b)^2$. Therefore, this model yields a parabolic threshold shape for the I_c-V spectrum. Although the above phase space restrictions are appropriate only if the CBM is located at k_t = O, *off-axis* minima may also be treated.

BEEM spectra have usually been obtained with the *STM* operating at constant I_t, which normalizes I_c and linearizes the BEEM spectrum. Equation (4) for I_c depends on tip-sample spacing s, which changes with V at constant I_t. Therefore Equation (4) will not describe an entire I_c-V spectrum. This effect has usually been modeled by treatings as a constant so and normalizing $I_c(s_0, V)$ by $I_t(s_0, V)$ for each voltage. This is usually a good

approximation and requires only that the tunnel distribution be insensitive to small changes in s. A modified expression for I_c may thus be written as

$$I_c = RI_{t0}\frac{\int_{E_x min}^{\infty} dE_x D(E_x)\int_0^{E_t max} dE_t[f(E)-f(E+eV)]}{\int_0^{\infty} dE_x D(E_x)\int_0^{\infty} dE_t[f(E)-f(E+eV)]} \quad 5.$$

where I_{t0} is the constant tunnel current at which the BEEM spectrum is measured. Note that, for spectra obtained under open-loop conditions, s is strictly constant and Equation (4) is used.

This kinematic model assumes that all electrons incident on the interface within the allowed phase space are collected. This classical assumption is not appropriate for abrupt interfaces. In this case the integrand of Equation (5) may be multiplied by the quantum-mechanical transmission factor $T(E,\mathbf{k})$ appropriate to the potential profile of the interface. For a step potential, this factor maybe written as[13]

$$T = \frac{4\frac{k_{xi}}{m}\frac{k_{xf}}{m_x}}{\left(\frac{k_{xi}}{m}+\frac{k_{xf}}{m_x}\right)^2} \quad 6.$$

Here, k_{xi} and k_{xf} are the normal components of the electron wave vector in the base and collector, respectively, and m_x is the component of semiconductor effective mass normal to the interface.

It is also possible to probe hole transport through materials and valence band structure at an interface. [14] By biasing the tip positively, electrons tunnel from the sample, creating a hole distribution in the base. A p-type semiconductor may then serve as a collector of these ballistic holes. The peaking of the hole distribution toward the base Fermi level introduces an asymmetry between the ballistic electron and hole spectroscopes. In electron BEEM, the higher-energy portion of the hot electron distribution is collected, where the distribution is maximum. For holes, the tail of the distribution is collected. The threshold behavior of the hole I_c-V spectrum, however, is the same as for the case of electrons, with a $(V-V_b)^2$ dependence.

Another implementation of BEEM, which maybe referred to as reverse-bias BEEM, provides a direct spectroscopy of electron and hole scattering, [15] The process may be illustrated using a p-type semiconductor. With a negative bias (-V) on the tip, electrons are injected into the base. Although these electrons are not collected by the p-

type semiconductor, they can scatter off the Fermi sea in the base, exciting secondary electrons to states above E_F. The holes that are thereby created may act in the same manner as holes injected by a positively biased tip, although with a different energy and angular distribution. Those holes that have energy $E < E_F - eV_b$ and satisfy phase space requirements may be collected, resulting in a spectrum with threshold dependence $(V - V_b)^4$. The model for this process is discussed in detail elsewhere. [9, 15] An analogous process occurs for hole injection, secondary hot electron creation, and collection with an n-type semiconductor. The same $(V - V_b)^4$ threshold dependence is found for this case.

REVIEW OF THE WORK

Early Work

The original applications of BEEM were to the Au/Si(100) and Au/GaAs(100) interface systems. [7] Si is a well-understood device material and has a surface which can easily be cleaned and passivated.[16] In addition, the Au/Si Schottky barrier height (SBH) is large, allowing low-noise measurements. BEEM spectra for this system agree well with the original theoretical model, [8] providing encouragement that the basic treatment assumed in the model was valid.

GaAs has a more complicated chemistry, and the conduction band structure near the Fermi level is more complex than for Si. The multiple band minima of GaAs introduce multiple thresholds in the spectrum. Extracted values from a fit to a three-threshold model agree well with the known Schottky barrier, which is determined by the position of the Γ minimum at the M/S interface, as well as with the known energies of the L and X minima with respect to the Γ minimum.[17]

Interface imaging was also performed on these two systems. [7, 18] Uniform interface transmission was observed for Au/Si in the form of spatially uniform BEEM current. Au/GaAs interfaces presented a distinctly different picture, with a large degree of heterogeneity for I_c. The observation of Ga appearing at the Au surface, together with the insolubility of As in Au, led to the conclusion that As island formation at the interface was the source of this non-uniformity. Additional experiments utilized a 2-monolayer AlAs diffusion barrier between the Au and GaAs.[18, 19] In this case, interface uniformity comparable to that of Au/Si was observed, confirming this conclusion,

The dependence of I_c on Au thickness was also measured.[18] This provides a measure of attenuation length λ for hot electrons in Au, a quantity for which there was considerable disagreement. [10, 20, 21] Many spectra were obtained for several different Au thicknesses, and the spectral intensities for each thickness were averaged together.

The results agreed with the simple form $I_c \propto e^{-t/\lambda}$, where t is the metal thickness. λ was determined to be 13 nrn for Au at an energy of about 1 eV above the Fermi level. [9, 18] Further investigation of the transport properties of hot electrons through metals and semiconductors has developed into one of the most fruitful areas of BEEM research.

Schottky Barrier Height Measurements

One emphasis of BEEM measurements has been the determination of SBH for various M/S systems. Ballistic-hole spectroscopy was applied to Au/p-Si barriers at 77K by Hecht and coworkers,[14] yielding a SBH of 0.35 eV in good agreement with other measurements. Au/GaAs hole barriers were also probed, and the light and heavy hole bands were resolved. To date, BEEM involving hole transport has not been exploited, primarily due to the added experimental requirement of low-temperature operation, due to the generally low SBH and the resultant larger leakage current noise.

Figure 2 shows BEEM measurements by Ludeke and coworkers for a series of metals evaporated on n-GaP(11O) cleaved in ultra-high vacuum (UHV). [22-26] While finding uniform SBH for each metal, they observed variations in BEEM intensity which they ascribed to the metal surface topography. Implications of this relative to scattering will be discussed below. They observed some spectra with anomalous shape and threshold position[25] which they attributed to the effects of tip contamination. Other III-V work was performed by Tsau and coworkers on the epitaxial CoGa/n-GaAs(100) system.[27] Here, the L and X minima were observed in the BEEM spectrum, but the Γ threshold, corresponding to the SBH, was not observed. It was hypothesized that the intensity of this minimum was too small to be resolved at existing signal-to-noise levels. However, an extrapolation downward by the known Γ-L separation yielded a SBH in agreement with other measurements. SBH's for the PtSi/n-Si(100) system have obtained by Niedermann and coworkers,[28] with the median value of 0.89 eV agreeing with that from conventional measurements. In addition, a dependence of SBH on PtSi thickness was reported[28] that has also been observed by conventional *I-V* techniques. [29] Coratger and coworkers[30] obtained BEEM results for the Au/n-ZnSe interface, They observed a large range for SBH, the lowest values of which agreed with conventional *I-V* measurements. They interpreted this variation in terms of microclusters of different ZnSe phases at the interface.

The high spatial resolution of BEEM has provided the first opportunity to characterize the lateral variation of SBH at a M/S interface. Fowell and coworkers investigated SB formation at the Au/CdTeintetiace,[31, 32] obtaining the first mapping of SBH at this M/S interface, with a range of more than 0.4 eV. In addition, they experimentally confirmed the three-threshold structure of Au/GaAs BEEM spectra.[32] In the work involving PtSi mentioned above,[28] SBH was also mapped laterally, although the large range observed seemed to be inconsistent with conventional *I-V*

measurements. Hasegawa and coworkers[33] attempted to resolve a change in SBH across an A/B boundary in the $NiSi_2$/Si(111) system, but observed only minor differences in the BEEM spectra. Mapping of other SBH variations has been reported by Palm and coworkers for Au/Si(100),[34] and by Talin and coworkers for Au/GaAs(100)[35] and Au/PtSi/Si(100).[36]

Davies and coworkers[37] performed the first BEEM measurements utilizing a biased sample. BEEM spectra were obtained as a function of reverse bias on a Au/Si Schottky diode. They measured the change in barrier lowering with voltage, obtaining good agreement with calculations (Figure 3). They also compiled data on the agreement between experimental spectra and the phase space BEEM model. [8) This agreement improved with increasing reverse bias, which they interpreted as a decrease in the effect of electron backscattering on the BEEM spectrum.

BEEM Threshold Behavior

The original kinematic model for BEEM spectroscopy[8] did not include scattering or dynamical effects such as QMR at the M/S interface. Schowalter and Lee[38] performed experiments on Au/Si(111) which yielded spectra remarkably similar to those of Au/Si(100). This would not be expected in the absence of scattering, since tunneling from the STM tip strongly weights the incoming electrons in the forward direction. The calculated threshold dependence for Si(111) would deviate strongly from quadratic, being determined by the overlap of the Si bared minima with the momentum tail of the tunneling distribution. Schowalter and Lee[38] performed Monte-Carlo calculations which included elastic scattering in the base and found good agreement with both Si(100) and Si(111) data, as shown in Figure 4.

With the addition of QMR, which has a leading order $(V - V_b)^{1/2}$ term, the threshold dependence becomes $(V - V_b)^{5/2}$. Similar treatments have been followed in the past with internal photoemission experiments, with excellent agreement of theory with experiment for both power laws. Prietsch and Ludeke proposed the 5/2 power dependence for BEEM thresholds.[22] Although they found excellent agreement with experiment in the threshold region for both models, there was a small systematic difference in threshold values between the two. Lee and Schowalter[39] presented calculations of both QMR and optical phonon backscattering in the semiconductor. This work indicated that the energy dependence of the two contributions largely canceled, leaving only a constant scaling factor. It should be noted also that the additional 1/2 power contributed by QMR would be present for reverse BEEM as well,[24] modifying the $(V - V_b)^4$ threshold dependence to $(V - V_b)^{9/2}$.

The most careful study addressing this question to date has been done by Henderson and coworkers.[40] In the first BEEM experiments below 77K, they performed measurements on Au/Si(100) with high signal-to-noise. The results were

compared both to the quadratic model and to a model using the 5/2 power law, and incorporating Si band non-parabolicity. By fitting the data to both models and examining the residuals, it was determined that the 5/2 power maintained a near-zero residual to significantly higher voltages than the quadratic model.

Epitaxial Systems and the Effects of Metal Band Structure

For M/S systems in which the metal layers are evaporated, heir polycrystallinity appears to diminish the effects of the metallic band structure on the BEEM spectra. Possible causes are elastic scattering within the layer by grain boundaries and other defects,[41] and scattering due to symmetry breaking at the non-epitaxial interface. However, BEEM spectroscopy has been reported for epitaxial systems where the electronic structure of the metal layer plays a role. Conventional measurements of $NiSi_2$/n-Si(1 11) have reported the presence of two discrete barrier heights of 0.65 eV and 0.79 eV for type A and B interfaces, respectively .[42] BEEM measurements on this system by Fernandez and coworkers[43] yielded values of 0.71 eV and 0.84 eV. In addition, the BEEM intensity was found to differ for the two types of interface. Hasegawa and coworkers,[33] in the work mentioned previously, performed UHV STM and BEEM onNiSi2/n-Si(111). They were able to determine local interface type by the orientation of silicide trimers and were able to localize the tip at A/B domain boundaries. These measurements did not yield a significant difference between BEEM thresholds or intensities for A and B regions. This was attributed to field pinching[44, 45] across the type-A domains, since the Debye length for the semiconductor was larger than the domain size.

Stiles and Hamann calculated theoretical BEEM spectra[46, 47] for $NiSi_2$/n-Si(1 11) using an ab initio method[48] to determine interface transmission probabilities. Their results yield spectra for A- and El-type interfaces which differ in intensity by a factor of three. Further structure in the spectra also appears due to details of the $NiSi_2$ band structure, which has not been convincingly demonstrated experimentally, perhaps due to scattering in the silicide.[47, 49]

The $CoSi_2$/n-Si(1 11) interface is also thought to have interesting properties which are produced by the silicide electronic structure. Mattheiss and Hamann[50] calculated the band structure for $CoSi_2$, and the results indicate the presence of an energy gap for values of k_t appropriate for transport into the CBM of Si(11 1). The presence of this gap would be expected to preclude the transport of electrons across the $CoSi_2$/Si interface until electron energy is well in excess of the SBH. However, conventional measurements yield the expected barrier height, [51-53] a situation that is not completely understood. Kaiser and coworkers[54] performed BEEM on $CoSi_2$/n-Si(1 1 1) samples at 77K. Their results yielded spectra, such as the one in Figure 5, exhibiting a threshold which was delayed by about 0.2 eV. Stiles and Hamann[55] generated theoretical $CoSi_2$/n-Si(1 11) BEEM spectra using the calculated band structures, and their results also produced a

BEEM threshold delayed by 0.2 eV. Their phase-space calculations for this interface are shown in Figure 6. It is possible that conventional measurements which integrate over large areas are dominated by defective regions, or perhaps by secondary electron production at the M/S interface. [54] Subsequent UHV measurements of BEEM spectra on $CoSi_2$/n-Si(1 11) by Sirringhaus and coworkers[56-58] did not reveal a delayed threshold; the discrepancy between the two experiments has not been adequately explained.

In work described above, Tsau and coworkers[27] have obtained BEEM spectra for CoGa/GaAs(1 00) which display thresholds at L and X of GaAs. The strong intensity of the X threshold relative to that of L is explained in t erms of the CoGa band structure, where CoGa states that cinematically match into the L minima of GaAs are not of L symmetry.

Transport and Scattering

Hot-electron transport characterization has developed into one of the most exciting areas for the application of BEEM. The first BEEM measurement involving a characterization of scattering was the determination of attenuation length in Au mentioned above. [18] Subsequently, the implementation of reverse BEEM provided a means to characterize electron-electron scattering in materials.[15] The work on Si(1 11) by Schowalter and Lee[38] represented the first attempt to numerically include elastic scattering in the BEEM formalism. Ludeke and coworkers[26] included an energy-dependent mean-free path in the BEEM model, based on the conductivity mean-he path and an inelastic mean-free path for electron-electron scattering. They were able to model the inflection of BEEM spectra for metals on GaP(1 10) at $(V - V_b) > 0.5$ V. The effect on I_c of quasi-elastic scattering by optical phonons in Si was treated by Lee and Schowalter.[39] Hallen and coworkers[49] modified the original BEEM model to include a function which contained the effects of energy-dependent interface transmission and energy-dependent scattering. Interface modification (to be discussed more fully later) was also related to inelastic scattering in Au/Si(111) by Hallen and coworkers. [59-61] McNabb and coworkers[62] observed a decrease in transmitted current in areas of Au/GaAs(1 00) samples subjected to ion-beam implantation. They invoked increased defect scattering to explain the decrease.

Further BEEM measurements of attenuation in Au have been made. Palm and coworkers[63] confirmed the low-energy value first measured by BEEM. [18]Ventrice and coworkers[64] performed experiments on Au at 77K and room temperature, the results of which are reproduced in Figure 7. They obtained λ= 13.3 nm at room temperature and λ= 14.7 at 77K. The weak temperature dependence is attributed to the predominance of defect scattering in the Au layer. Interestingly, the zero-thickness extrapolation of BEEM intensity yields a ratio of $\lambda(77K)/\lambda(293K)$=1.79. This relatively

stronger temperature dependence is correlated with the quenching of the transverse acoustic phonon population in Si at low temperature. Attenuation lengths have also been measured in other materials. Niedermann and coworkers determined attenuation lengths in PtSi. [28, 65] Their measurements yielded λ=4.0 nm for thinner layers and λ=9. 1 nm for thicker layers, the difference being tentatively assigned to the presence of a disordered or defective layer up to 15 nm thick. The first BEEM measurement of attenuation length in $CoSi_2$ by Lee and coworkers[57] produced a 77K value of 7.1 nm at low energies. They subsequently obtained the energy dependence of attenuation length,[66] and were able to measure a difference in the value as a function of silicide orientation. This first BEEM measurement of the orientation dependence of attenuation length in a metal was attributed to an orientation dependence of electron group velocit y and intervalley scattering.

Ludeke and Bauer[67, 68] performed BEEM attenuation length measurements on Pd/Si structures. By using base layers as thin as 0.8 nm, and comparing spectra for varying Pd thickness to a scattering model, they obtained values for inelastic and elastic mean-free paths separately as a function of energy in the range 1 - 5 eV (Figure 8). They attributed the independence of BEEM current on Si substrate orientation to interface scattering. As with the results of Lee and coworkers on $CoSi_2$,[66] their measurement of energy-dependent mean-free-path showed a large deviation from theory.

Lee and Schowalter[69] observed peaks in the derivatives of Au/Si(100) BEEM spectra, which they attributed to inelastic events. They consistently observed a sharp maximum in the derivative at 1.04 eV, which they assigned to the onset of phonon-assisted exciton creation at the Au/Si interface. They also observed other peaks in the derivative, the unambiguous assignment of which was complicated by some degree of spatial variation.

An early gauge on the degree of scattering in the metal layer was observed by Prietsch and Ludeke[22] for various metals on cleaved GaP(1 10). They imaged local decreases in interface transmission over areas in which the surface gradient was large relative to the metal/GaP interface. This "searchlight" effect was attributed to the deflection of the tunneling distribution away from the interface normal by a locally sloping surface, thereby decreasing current into the GaP conduction-band minimum at k_t=0.[70] This searchlight effect was not seen by Schowalter and coworkers on Au/Si(100) samples. [71] They more recently reported occasional observation of the effect using PtIr tips with a sharper radius of curvature than previous Au tips.[64]

A related test of scattering involves a quantitative measure of BEEM imaging resolution, Schowalter and Lee performed Monte-Carlo calculations[38] of scattering in BEEM, using the values λ_{el}=1 O nm, and λ_{inel}=120 nm. Their estimates of spatial resolution for a 10 nm Au layer were about 18 nm for Si(l 00) and 35 run for Si(l 11). Davies and coworkers[72] performed BEEM imaging on Au(1 1 nm)/SiO_2/SiGe(100) structures where the SiO_2 had been patterned by wet etching. Line scans of topography

and BEEM current at the edge of a hole in SiO_2 showed that the BEEM current was attenuated over a length scale of several nm as the tip moved over an oxide edge. Further detailed measurements were performed for Au(I 5nm)/SiO_2/Si by Milliken and coworkers[41] on both Si(1 00) and Si(11 1). Results are shown in Figure 9. Derived BEEM widths as the tip scanned over an oxide edge were between 1.0 andl .5 nm. Monte Carlo simulations including both bulk and interface scattering were unable to reproduce these narrow widths while at the same time providing the large transmitted currents experimentally observed for the Si(111) case. [38] Grain boundary confinement was proposed as one possible mechanism to explain the high resolution.

Attenuation lengths *in* semiconductors have also been measured using BEEM techniques. Bell and coworkers[73, 74] performed BEEM measurements on Au-covered Si(1 00) pn junctions grown by molecular-beam epitaxy (MBE). in these experiments, BEEM spectroscopy was used to characterize samples with varying p-layer thicknesses. The attenuation of I_c was measured as a function of p-layer thickness at both room temperature and 77K. These measurements yielded λ_{Si}=45 nm at room-temperature. Unexpectedly, a value of 24 nm was obtained at 77K. A possible mechanism involving inter-valley scattering in the Si was proposed to explain the results.

Transport and scattering processes at higher energies has also been an area of recent BEEM emphasis. Ludeke was the first to apply BEEM at injection voltages in excess of 3 V.[75, 76] He observed structure in BEEM spectra of Cr/GaP which showed a convincing correspondence to GaP density-of-states structure, as shown in Figure 10. He demonstrated that collector current can exceed injected current at these high electron energies, due to impact ionization and carrier multiplication. Bauer and Ludeke performed further expenments[78, 79] using a thin $NiSi_2$ base layer with pinholes. By utilizing BEEM spectroscopy over the pinholes on the bare Si(111)-(7x7), the effective base electrode thickness was quite small, and quantitative comparison with models for scattering in the Si could be made. As Figure 11 shows, they found excellent agreement with recent theoretical treatments of impact ionization.[80, 81] Bauer and coworkers[82, 83] performed UHV BEEM experiments on GaP(1 10) using Au or Mg as the base metal. Using Monte-Carlo methods, they were able to include ballistic transport, elastic and inelastic scattering, and impact ionization in their theoretical calculations. They obtained excellent agreement with experimental BEEM spectra up to 6 eV, for a wide range of metal thicknesses and BEEM spectral shapes,

Since scattering of electrons by defects depends fundamentally on the atomic-scale structure of the material, the high spatial resolution of BEEM makes it an ideal tool for the investigation of defect scattering, Fernandez and coworkers[84] imaged local areas of heightened transmission in $NiSi_2$/Si(1 11) structures, which they attributed to increased elastic scattering by defective areas. Sirringhaus and coworkers, [56-58] in a series of experiments using a low temperature UHV BEEM apparatus, were able to image individual interface dislocations in the $CoSi_2$/Si(1 11) system. Their images are reproduced

in Figure 12. Scattering by these dislocations serves to increase the population of electrons at the large k_t of the Si minima, thus increasing transmitted current. They also observed a difference in BEEM spectra over dislocations versus spectra away from the dislocations.

Structure in BEEM spectra indicative of coherent electron transport also provides information about the degree of scattering. Sirringhaus and coworkers[56-58, 85] observed fluctuations in BEEM spectra of $CoSi_2$/Si(111) which they assigned to the presence of standing waves in the silicide. They were also able to map the spatial variation of silicide thickness with atomic resolution using the quantized changes in BEEM current. [86] Sajoto and coworkers observed quasi-bound states in III-V heterostructures, [87] which will be more fully discussed below.

Interface Modification

BEEM has also been used to study modified interfaces. Some of the first work in this area, described above, was the use of a thin AlAs layer as a diffusion barrier in the Au/GaAs system by Kaiser and coworkers.[18, 19, 88] Talin and coworkers used a native oxide barrier on GaAs[89] to prevent diffusion, which also had the effect of lengthening the sample lifetime.

Quattropani and coworkers[90] used BEEM to examine the effect of a RF-plasma cleaning of the Si surface on PtSi/Si(100) interface properties. They found that SBH decreased with this treatment, which they proposed was due to the increase in near-interface defect density, producing a large fixed charge accumulation near the interface which lowered the Schottky barrier. Davies and coworkers[72, 91] investigated the effect of reactive-ion etching of SiGe substrates by performing BEEM measurements of Au/SiGe structures. They found a statistically significant decrease in SBH in these areas compared with unetched areas. McNabb and coworkers[62] also examined the effect on BEEM spectra of ion-beam damage in Au/GaAs diodes. They observed a large decrease in interface transmittance, which they attributed to enhanced scattering from the ion-induced defects. Everaert and coworkers[92] observed a large increase in SBH of Au/GaAs due to mechanical polishing of the GaAs substrate, attributed to removal of Fermi-level pinning by hydrogen passivation of defects.

Diffusion also occurs at the Au/Si interface. There have been many studies of this process, [93-95] which appears to proceed via the formation of an intermediate Au silicide. [96] Fernandez and coworkers[59] reported a lack of BEEM current for Au deposited on a UHV-cleaned Si surface and proposed enhanced Au/Si interdiffusion as the cause. They speculated that chemical surface treatments used to clean the Si surface in previous BEEM experiments[7, 14, 15] left behind trace contaminants which served as a partial barrier to diffusion. Bell and coworkers observed interdiffusion between Au and

strained SiGe, which produced a roughened Au/SiGe interface and heterogeneous strain in the SiGe layer. [97-99]

Fernandez and coworkers[59] reported the first interface modification studies using BEEM as the source of the modification. They found that an irreversible decrease in I_c occurred upon application of high tip voltage (3 -4 V) in Au/Si samples. Using BEEM imaging they discovered that this produced an area of several tens on nm under the STM tip where transmittance was reduced. They sometimes observed this area to be surrounded by a boundary of increased transmittance. A topographic change was also often observed. Subsequent work[61] demonstrated that interface modification could be achieved using more modest voltages (< 2.5V) which did not alter the surface topography and which enhanced transmittance. Examples of both of these cases are given in Figure 13. They developed a microscopic model for the modification process which included time dependence.[61]

In contrast to these experiments, Cuberes and coworkers[100, 101] obtained BEEM spectra for Au deposited in situ on Si(111)-(7x7). They were able to obtain high-quality spectra which showed no irreversible behavior at high voltages. These results are perhaps due to a superior robustness of the (7x7) surface against dissociation in the presence of Au.

BEEM of Heterostructures

Several applications involving BEEM on multilayer heterostructures have been demonstrated. The earliest effort in this area was described by Shen and coworkers, [102, 103] where BEEM spectroscopy was performed on Au/InAs/GaAs. The BEEM threshold which they measured corresponded to the difference between E_F and the CBM in the GaAs. More recently Ke and coworkers[104] used BEEM to probe the uniformity of both strained and relaxed InGaAs/AlAs interfaces. They found that a partially relaxed InGaAs layer produced a wide range in SBH (> 0.25 eV), while the fully strained case displayed more uniform barriers (< 0.1eV variation).

The work mentioned above by Bell and coworkers on Si pn junctions[73, 74] represented an example of BEEM on multilayer structures. Kaiser and coworkers followed the early efforts using AlAs as a diffusion barrier on GaAs[18] with a study of electron transmission through AlAs/GaAs heterostructures as a function of AIAs thickness. [105] They were able to track the changes in transmission up to the point where the AlAs layer was opaque to electrons. Figure 14 shows this series of spectra. For the thickest AlAs layers, they were able to measure the AlAs L-X splitting, a value recently reproduced by Ke and coworkers. [104] O'Shea and coworkers[106] obtained BEEM spectra for single-barrier GaAs/AlGaAs/GaAs heterostructures from which they derived the band offset for this system, Further work by Sajoto and coworkers[87] concentrated on a BEEM spectroscopy study of III-V double-barrier resonant tunneling structures

(DBRTS). These samples consisted of Au deposited on a five-layer GaAs/AlGaAs double barrier structure (Figure 15(a)). A buried p-type δ-doped layer was inserted to flatten the bands in the region of interest. In a series of measurements from 77K to room temperature, they obtained a family of spectra each of which produced peaks in the second derivative (Figure 16) that changed systematically with temperature. By comparing the results to calculations, they were able to assign the peaks not only to the positions of band edges, but also to the presence of quasi-bound states in the central GaAs well. These assignments are given in Figure 15.

Bell and coworkers performed BEEM spectroscopy on metal/SiGe/Si(100) heterostructures, mentioned above.[97] Using thin pseudomorphic SiGe layers, they were able to investigate the effects of strain on the SiGe band structure. With Ag as the base metal, they obtained values of the strain-induced conduction-band splitting in SiGe which agreed well with calculations. [107, 108] Au base layers produced interdiffusion, as discussed above, causing a roughening of the M/S interface and a heterogeneity of band splitting. A BEEM spectrum showing one of the larger observed splittings appears in Figure 17. Elastic modeling of this roughness produced a strain variation in good agreement with that derived from BEEM measurements of the band splitting.[99]

Other recent research has concentrated on metal/oxide/semiconductor heterostructures. Cuberes and coworkers[100, 109] used BEEM to study Au/CaF_2/Si(111)-(7x7). They obtained BEEM spectra with a threshold corresponding to the CaF_2 band edge and observed structure which they correlated with the CaF_2 density of states. Ludeke and coworkers[110, 111] performed experiments on Pt/SiO_2/Si(100). A BEEM threshold of 3.9 V marked the SiO_2 conduction-band edge, and they were able to extract a measure of oxide transmission probability after first removing contributions from impact ionization in the Si. They were also able to vary this transmission by applying a bias across the oxide and bending the bands, a technique introduced by Davies and coworkers.[37] A model emphasizing electron-phonon scattering was used to fit the voltage-dependent oxide transmission characteristics.

Other Recent Results

Other recent applications of BEEM techniques maybe mentioned. One of the most interesting recent results was shown by Sirringhaus and coworkers.[112-114] They performed imaging of $CoSi_2$ on Si(100) and Si(111) and observed BEEM images which reflected the atomic periodicity of the surface. A conventional BEEM image (Figure 18) and a reverse BEEM image (Figure 19) are shown for the (100) orientation. This periodicity in the BEEM images was explained in terms of the modulation of the tunneling distribution by the atomic corrugation of the surface. Using both conventional and reverse BEEM spectroscopy and imaging on both orientations of Si, they were able to determine that the modulation was primarily that of the energy distribution of tunneling, rather than the momentum distribution.

Kaiser and coworkers[115] presented initial work on a BEEM-related technique which they called tunneling transmission microscopy. In this experiment, an STM tip tunneled to a free-standing membrane which was suspended in vacuum, If the tunneling voltage exceeds the work function of the material and if the membrane is thin enough, some of the electrons pass through and exit the back side of the membrane, where they are collected. Meepagala and Baykul published the first results using thistechrique.,[116] with a threshold for transmission approximately equal to the work function of the material. Experimental challenges of this measurement include the flexibility of the membrane and the tendency of the biased STM tip to attract the thin film.

Finally, some information has appeared in the literature concerning experimental designs for BEEM measurements. Zhang and coworkers[1 17] have provided a method for adapting a conventional STM for BEEM measurements. They present a design for use in an ambient environment. Henderson and coworkers[118] describe a STM/BEEM system which is capable of very-low-temperat ure (<77K) BEEM measurements. This instrument is designed to operate in a liquid helium storage dewar, and has a very large in-situ coarse positioning capability.

SUMMARY

This survey has been intended as an introduction to many of the exciting new areas of research being pursued using BEEM techniques. The wide energy range accessible to BEEM spectroscopy and imaging enables investigations of many different problems. Due to its unique capabilities of high spatial resolution and injection of a controlled electron distribution, BEEM techniques will contribute to many other interface and transport investigations in the future.

ACKNOWLEDGMENT

The portion of this research which is by the authors of this review was performed by the Center for Space Microelectronics Technology, Jet Propulsion Laboratory, California Institute of Technology, and was jointly sponsored by the Office of Naval Research and the Ballistic Missile Defense Organization / Innovative Science and Technology Office"through an agreement with the National Aeronautics and Space Administration.

Literature Cited

1 Brillson LJ. 1982. *Surf. Sci. Rep.* 2:123-326, and references therein

2 Le Lay G, Derrien J, Boccara N. 1987. ***Semiconductor Interfaces: Formation and Properties.*** Berlin: Springer-Verlag, and references therein

3 Spitzer WG, Crowell CR, Atalla MM. 1962. *Phys. Rev. Lett.* 8:57-8; Crowell CR, Spitzer WG, White HG. 1962. *Appl. Phys. Lett.* 1:3-5

4 Seah MP, Dench WA, 1979. *Surf. Interface Anal.* 1:2-xx

5 Binnig G, Rohrer H. 1982. *Helv. Phys. Acts* 55:726-35

6 Stroscio JA, Kaiser WJ, eds. 1993. *Scanning Tunneling Microscopy. San* Diego: Academic Press

7 Kaiser WJ, Bell LD. 1988. ***Phys. Rev. Lett. 60:1406-09***

8 Bell LD, Kaiser WJ. 1988. ***Phys. Rev. Lett. 61:2368-71***

9 Bell LD, Kaiser WJ, Hecht MH, Davis LC. 1993. In ***Scanning Tunneling Microscopy,*** ed. Stroscio JA, Kaiser WJ, pp. 307-48. San Diego: Academic Press

10 Crowell CR, Spitzer WG, Howarth LE, LaBat e EE. 1962. ***Phys. Rev.*** 127:2006-15

11 Simmons JG. 1963. ***J. Appl. Phys. 34:1793-1803***

12 *Sze* SM, Crowell CR, Carey GP, LaBate EE. 1966. *J. Appl. Phys.* 37:2690-95

13 Gasiorowicz S. 1974. ***Quantum Physics,*** p. ***77. NY:*** John Wiley

14 Hecht MH, Bell LD, Kaiser WJ, Davis LC. 1990. ***Phys. Rev. B*** 42:7663-66

15 Bell LD, Hecht MH, Kaiser WJ, Davis LC. 1990. ***Phys. Rev. Lett.*** 64:2679-82

16 Grunthaner PJ, Grunthaner FJ, Fathauer RW, Lin TL, Hecht MH, et al. 1989. ***Thin Solid Films*** 183:197-212

17 Blakemore JS. 1982. ***J. Appl. Phys.*** 53:R123-81

18 Hecht MH, Bell LD, Kaiser WJ, Grunthaner FJ. 1989. *Appl. Phys. Lett.* 55:780-82

19 Kaiser WJ, Bell LD, Hecht MH, Grunthaner FJ. 1989. *J. Vat. Sci. Technol. B* 7:945-49

20 *Sze* SM, Moll JL, Sugano T. 1964. ***Solid State Electron.*** 7:509-23

21 Soshea RW, Lucas RC. 1965. *Phys. Rev.* 138:A1 182-88

22 Prietsch M, Ludeke R. 1991. *Phys. Rev. Lett.* 66:2511-14

23 Prietsch M, Samsavar A, Ludeke R. 1991. ***Phys. Rev. B 43:11850-56***

24 Ludeke R, Prietsch M. 1991. *J. Vat. Sci. Technol. A* 9:885-90

25 Prietsch M, Ludeke R. 1991. *Surf. Sci.* 251/252:413-17

26 Ludeke R, Prietsch M, Samsavar A. 1991. *J. Vat. Sci. Technol. B* 9:2342-48

27 Tsau L, Kuo TC, Wang KL. 1993. *Appl. Phys. Lett.* 63:] 062-64

28 Niedermann P, Quattropani L, Solt K, Kent AD, Fischer O. 1992. *J. Vat. Sci. Technol. B* 10:580-85

29 Solt K. 1990. ***Vacuum 41:827-30***

30 Coratger R, Ajustron F, BeauVillain J, Dharmadasa IM, Blomfield CJ, Prior KA, et al.)995. ***Phys. Rev. B*** 51:2357-62

31 Fowell AE, Williams RH, Richardson BE, Shen T-H. 1990. *Semicond. Sci. Technol.* 5:348-50

60 Hallen I-ID, Fernandez A, Huang T, Buhrman RA, Silcox J. 1991. *J. Vat. Sci. Technol. B* 9:585-89
61 Hallen HD, Huang T, Fernandez A, Silcox J, Buhrman RA. 1992. *Phys. Rev. Lett.* 69:2931-34
62 McNabb JW, Skvarla M, Craighead HG. 1994. *J. Vat. Sci. Technol. B 12:3712-15*
63 Palm H, Arbes M, Schulz M. 1993. *Appl. Phys. A Solids Surf. A56:* 1-7
64 Ventrice CA, LaBella VP, Ramaswamy G, Yu H-P, Schowalter LJ. 1995. *Phys. Rev. B.* In press
65 Niedermann P, Quattropani L, Solt K, Maggio-Aprile I, Fischer O. 1993. *Phys. Rev. B* 48:8833-39
66 Lee EY, Sirringhaus H, Kafader U, von Känel H. 1995. *Phys. Rev. B 52: 1 816-29*
67 Ludeke R, Bauer A. 1993. *Phys. Rev. Lett. 71:1760-63*
68 Ludeke R, Bauer A. 1994. J. *Vat. Sci. Technol. A* 12:1910-14
69 Lee EY, Schowalter LJ. 1992. *Phys. Rev. B* 45:6325-28
70 Prietsch M. 1992. *Habilitationsschrift*, Institut für Experimentalphysik, Freie Universität Berlin
71 Lee EY, Turner BR, Schowalter LJ, Jimenez JR. 1993. *J. Vat, Sci. Technol. B* 11:1579-83
72 Davies A, Couillard JG, Craighead HG. 1992. *Appl. Phys. Lett. 61:1040-42*
73 Bell LD, Manion SJ, Hecht MH, Kaiser WJ, Fathauer RW, Milliken AM. 1993. *Phys. Rev. B* 48:5712-15
74 Manion SJ, Milliken AM, Kaiser WJ, Bell LD, Hecht MH, Fathauer RW. 1994. *Proc. 4th Int. Conf. Form. Semicond. Interfaces, Julich*, pp. *711-18.* Singapore: World Scientific
75 Ludeke R. 1993. *Phys. Rev. Lett.* 70:214-17
76 Ludeke R. 1993. *J. Vat. Sci. Technol. A* 11:786-91
77 Chelikowsky JR, Chadi DJ, Cohen ML. 1973. Phys. Rev. B 8:2986-94
78 Bauer A, Ludeke R. 1994. *Phys. Rev. Lett. 72:928-31*
79 Bauer A, Ludeke R. 1994. J. *Vat. Sci. Technol. B* 12:2667-74
80 Alig RC, Bloom S, Struck CW. 1980, *Phys. Rev. B 22,5565-82*
81 Cartier E, Fischetti MV, Eklund EA, McFeely FR. 1993. *Appl. Phys. Lett.* 62:3339-41
82 Bauer A, Cuberes MT, Prietsch M, Kaindl G. 1993. *Phys. Rev. Lett.* 71:149-52
83 Bauer A, Cuberes MT, Prietsch M, Kaindl G. 1993. *J. Vat. Sci. Technol. B 11:1584-90*
84 Fernandez A, Hallen HD, Huang T, Buhrman RA, Silcox J. 1991. *Phys. Rev. B* 44:3428-31
85 *Lee* EY, Sirringhaus H, von Känel H. 1994. *Phys. Rev. B* 50:5807-09
86 Lee EY, Sirringhaus H, von Känel H. 1994. Phys. *Rev. B* 50:14714-17
87 Sajoto T, O'Shea JJ, Bhargava S, Leonard D, Chin MA, Narayanamurti V. 1995. *Phys. Rev. Lett.* 74:3427-30
88 Hecht MH, Bell LD, Kaiser WJ. 1989. *Appl. Surf. Sci. 41/42: 17-24*

89 Talin AA, Ohlberg DAA, Williams RS, Sullivan P, Koutselas I, Williams B, Kavanagh KL. 1993. *Appl. Phys. Lett.* 62:2965-67
90 Quattropani L, Solt K, Niedermann P, Maggio-Aprile I, Fischer O, Pavelka T. 1993. *Appl. Surf. Sci. 70/71* :391-95
91 Couillard JG, Davies A, Craighead HG. 1992. J. *Vat. Sci. Technol. B 10:3112-15*
92 Everaert JL, Van Meirhaeghe RL, Laflere WH, Cardon F. 1995. *Semicond. Sci. Technol.* 10:504-08
93 Molodtsov SL, Laubschat C, Shikin AM, Adamchuk VK. 1992. *Surf. Sci.* 269/270:988-94
94 Hanbucken M, Imam Z, Metois JJ, LeLay G. 1985. *Surf. Sci.* 162:628-33
95 Lamontagne B, Sacher E, Wertheimer MR. 1994. *Appl. Surf. Sci. 78:399-411*
96 Ma Z, Allen LH. 1993. *Phys. Rev. B* 48:15484-87
97 Bell LD, Milliken AM, Manion SJ, Kaiser WJ, Fathauer RW, Pike WT. 1994. *Phys. Rev. B* 50:8082-85
98 Bell LD. Milliken AM. Manion SJ, Kaiser WJ, Fathauer RW, Pike WT. 1995. *J.*

115 Kaiser WJ, Manion SJ, Milliken AM, Bell LD, Hecht MH. 1992. Tunneling transmission microscopy. ***Ballistic Electron Emission Microscopy Workshop*** pp. 18-20 (Abstr.)
116 Meepagala SC, Baykul MC. 1994. *Phys.* Rev. *B* 50:13786-88
117 Zhang R, Stefaniuk R, Ivey DG. 1995. Rev. ***Sci. Instrum.*** 66:3799-3801
118 Henderson GN, First PN, Gaylord TK, Glytsis EN, Rice BJ, Dantzscher PL, et al. 1995. ***Rev. Sci. Instrum.*** 66:91-96

1-

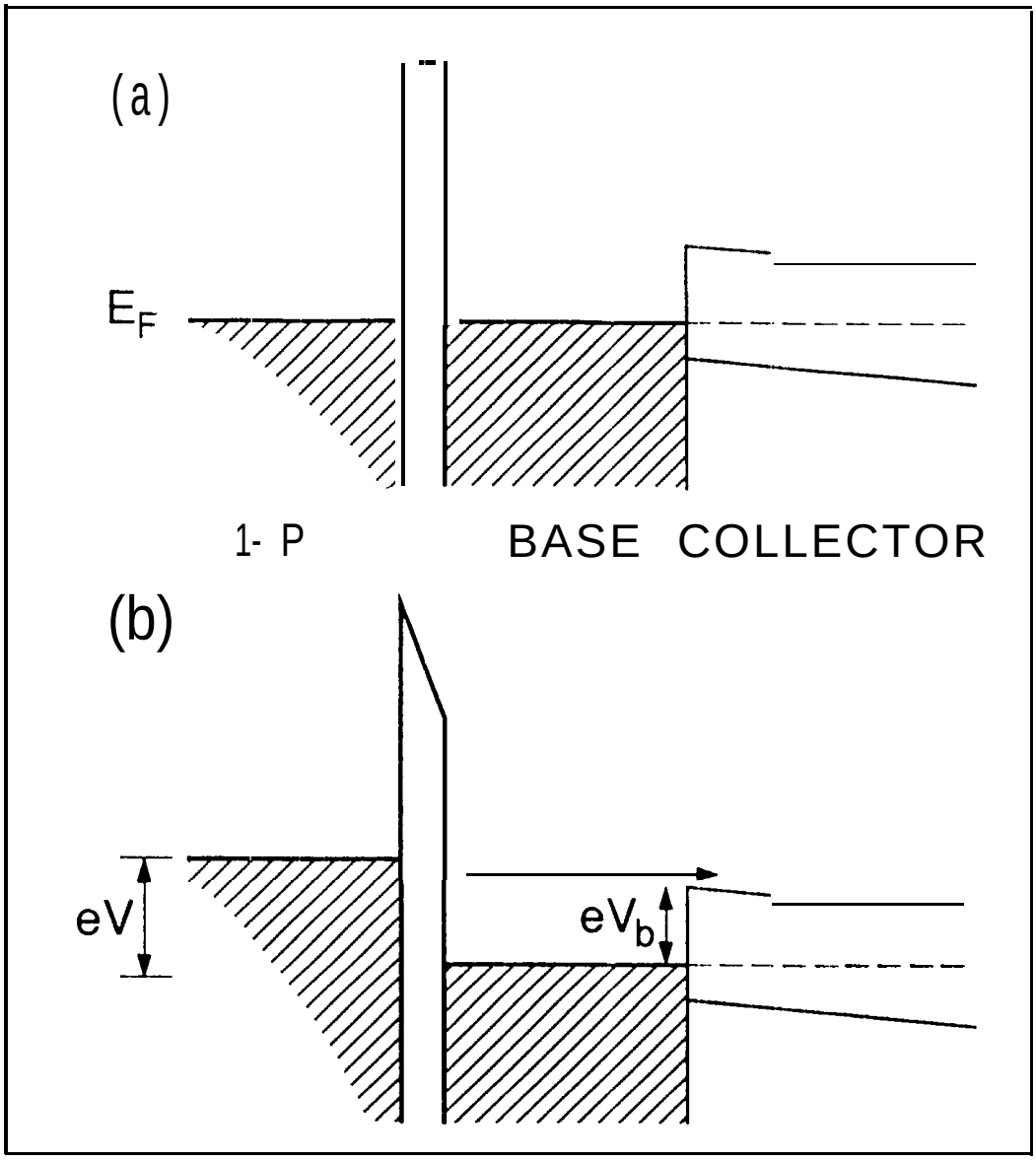

Figure 1
Bell and Kaiser
Arm. Rev. Mater. Sci.
Page 21

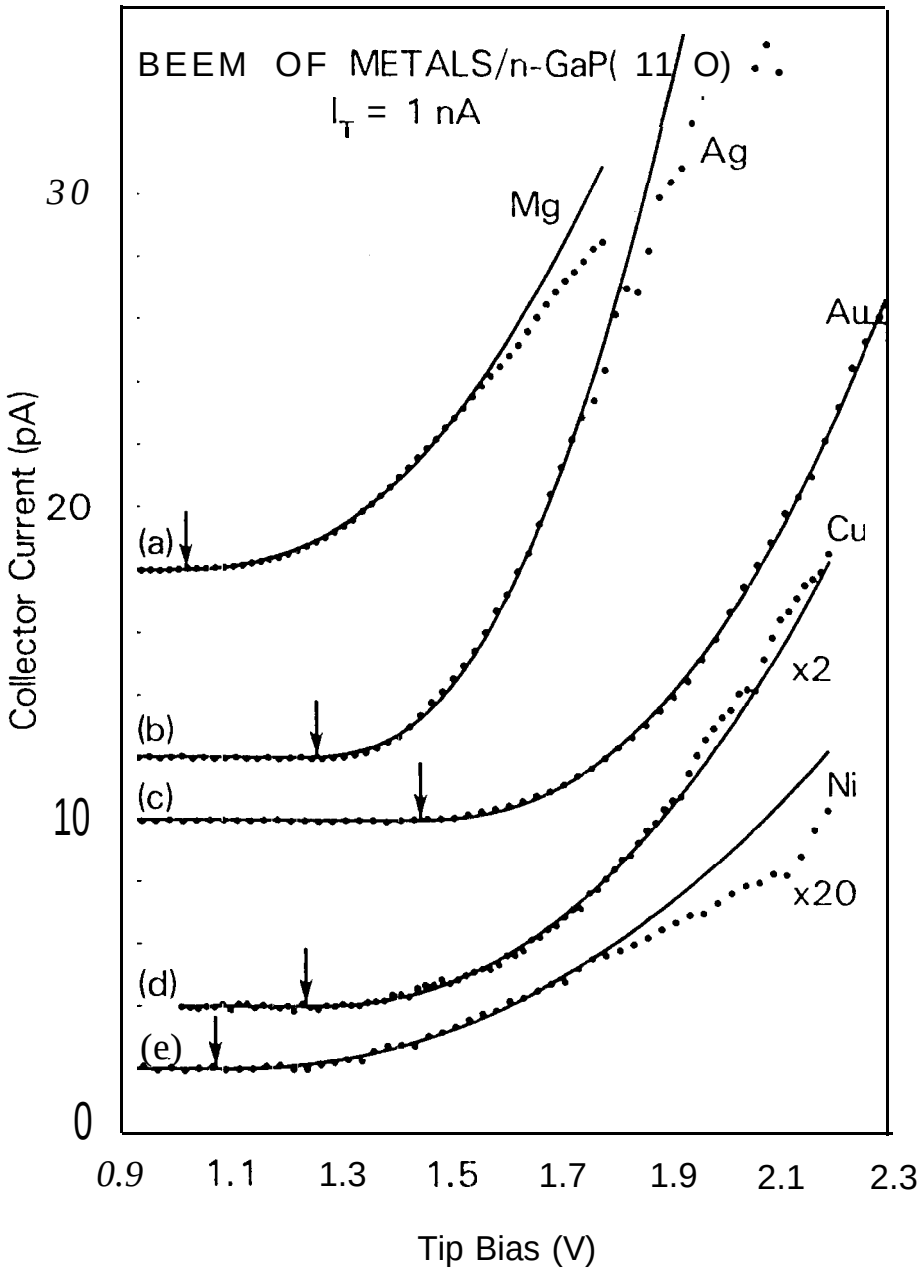

Figure 2
Bell and Kaiser
Ann. Rev. Mater, Sci.
Page 22

Fig 1

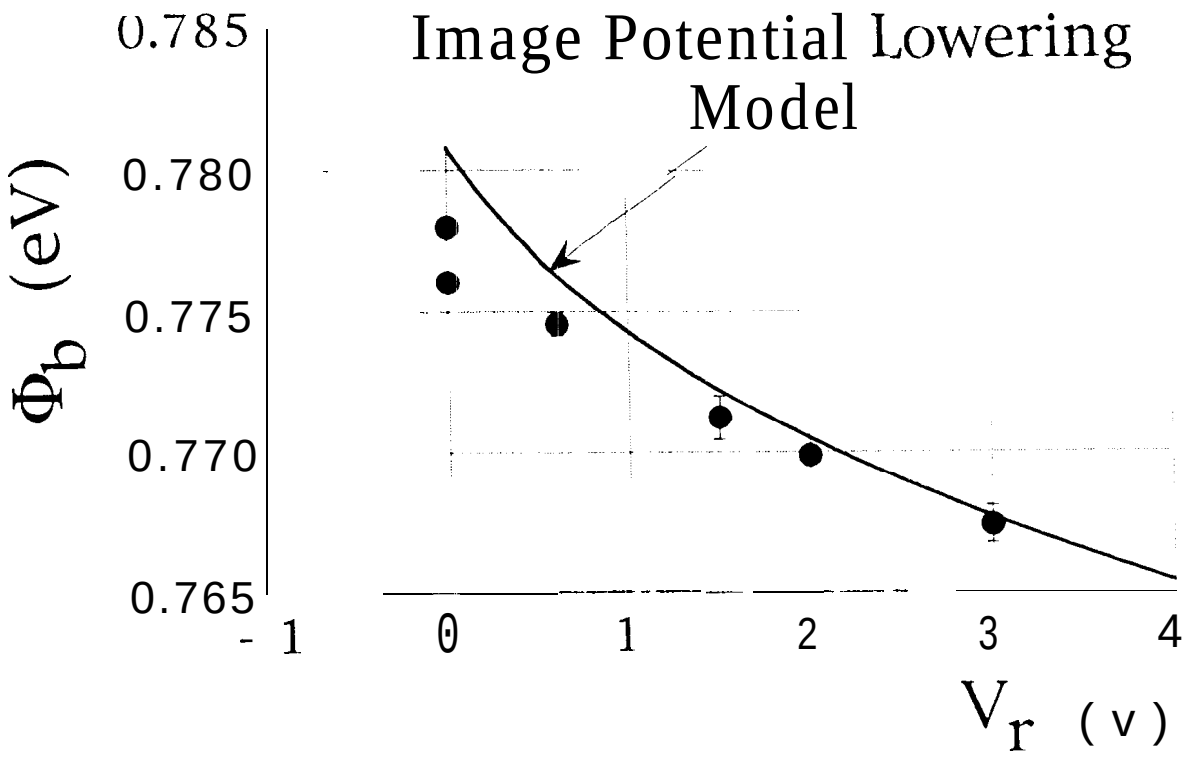

Figure 3
Bell and Kaiser
Ann. Rev. Mater. Sci.

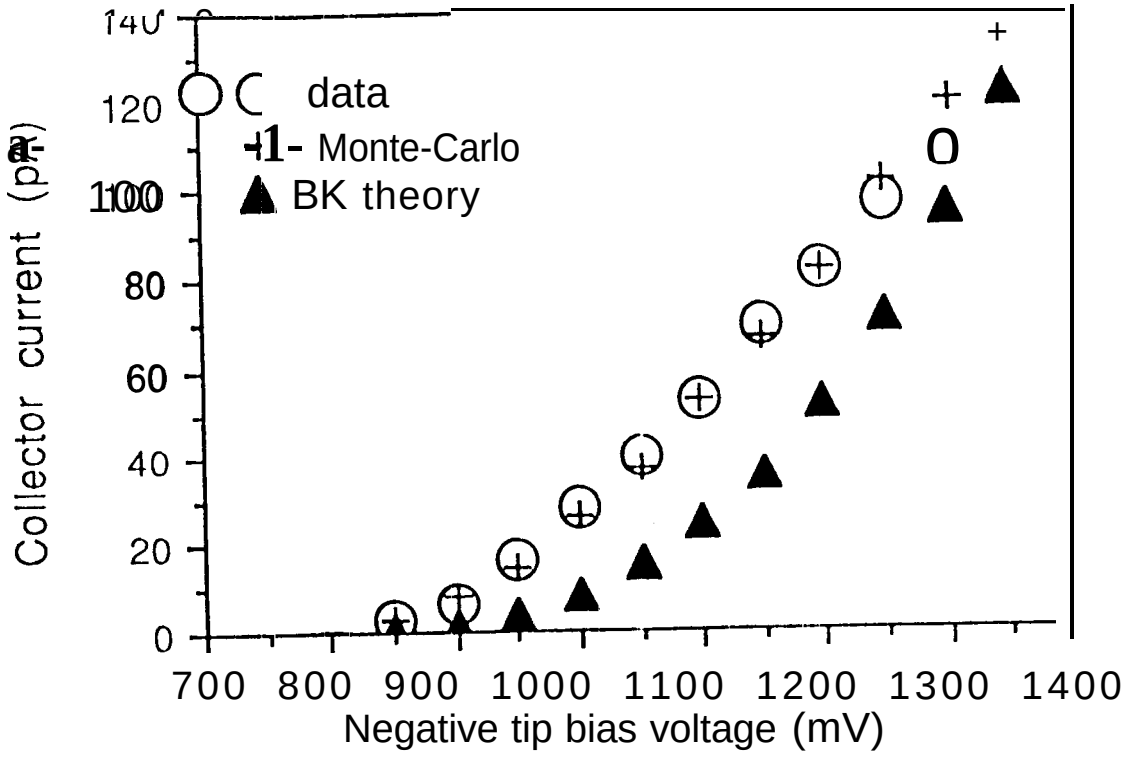

Figure 4
Bell and Kaiser
Ann. Rev. Mater. Sci.

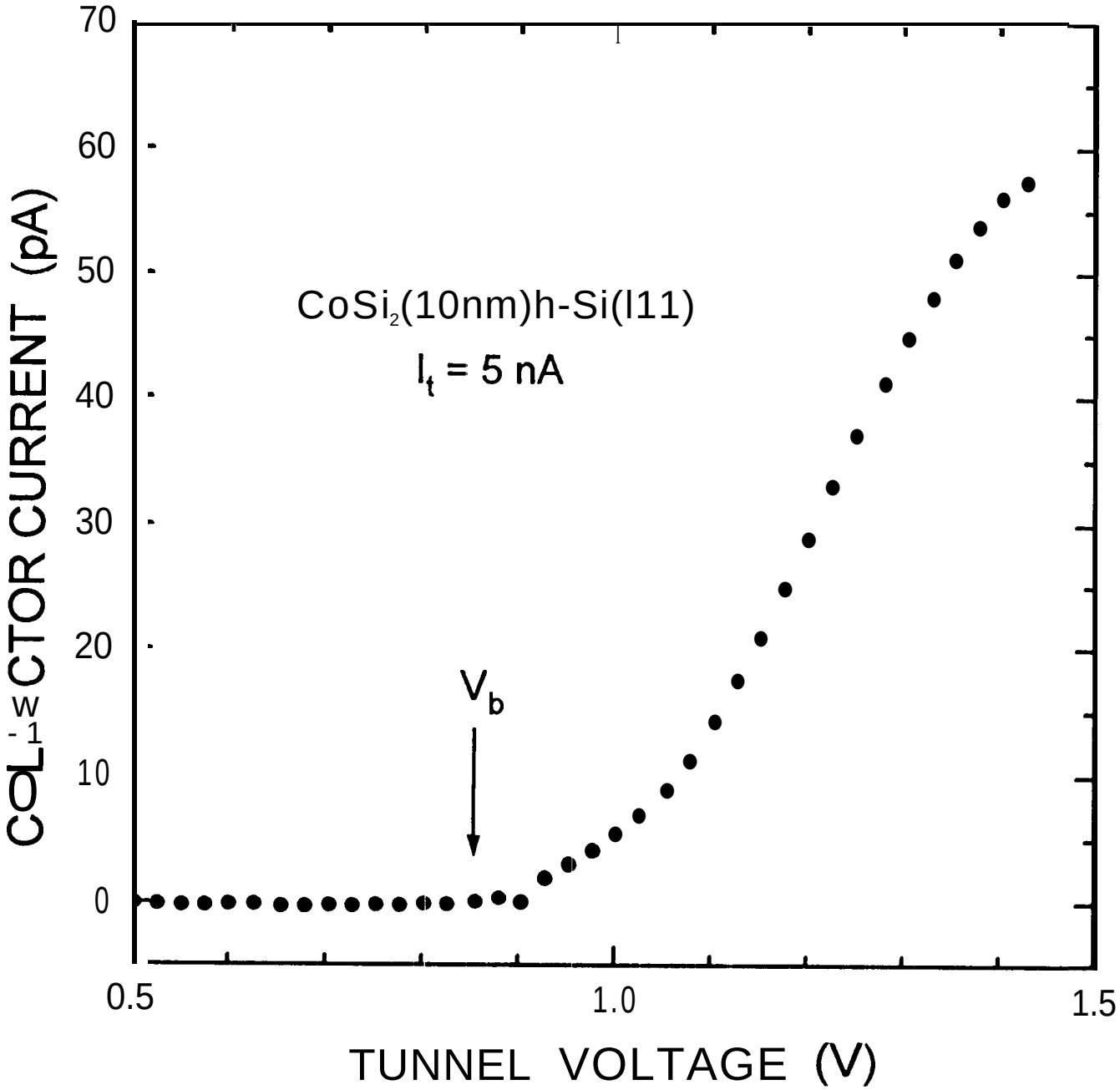

Figure 5
Bell and Kaiser
Ann. Rev. Mater. Sci.
Page 25

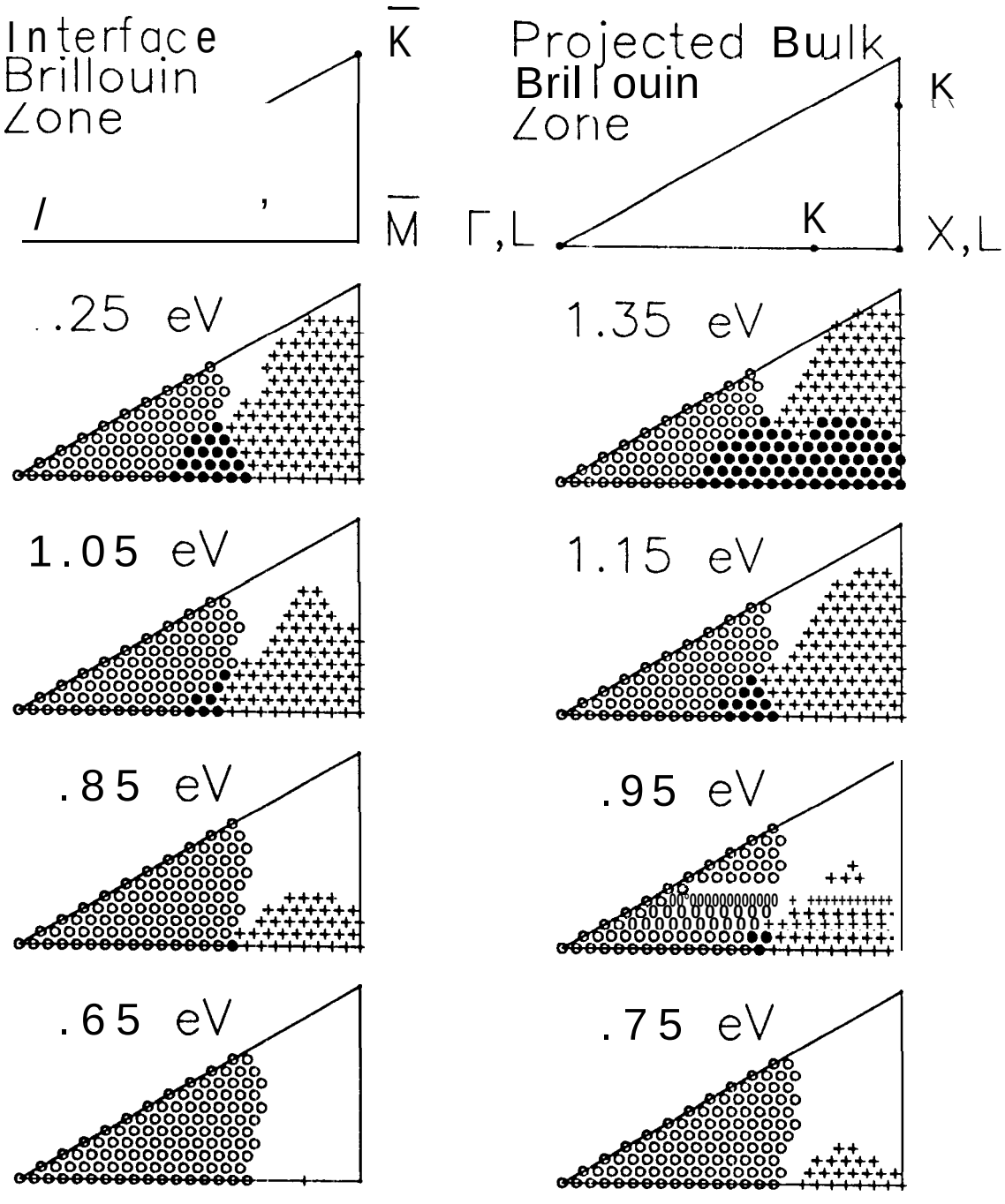

Figure 6
Bell and Kaiser
Ann. Rev. Mater. Sci.

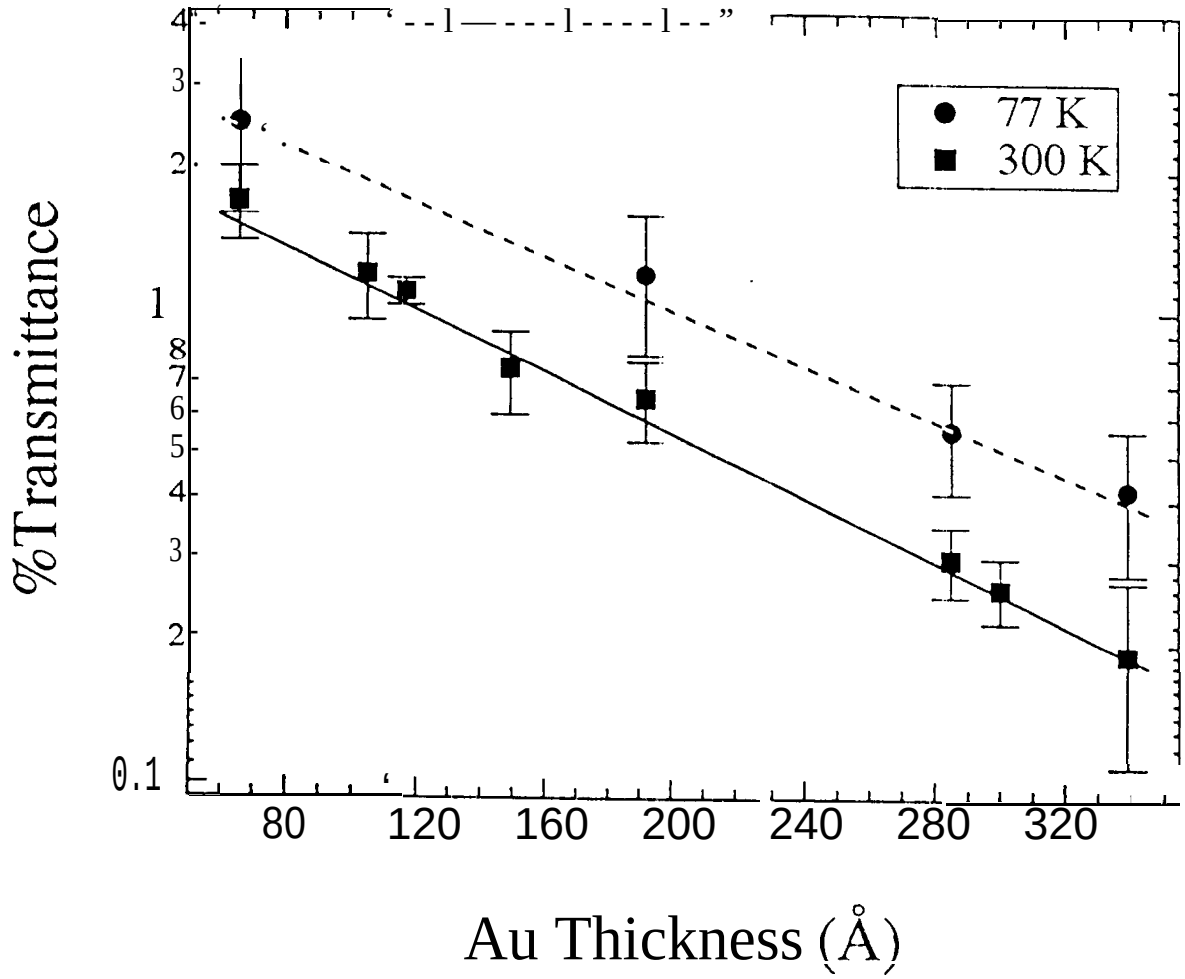

Figure 7
Bell and Kaiser
Arm. Rev. Mater. Sci.
Page 27

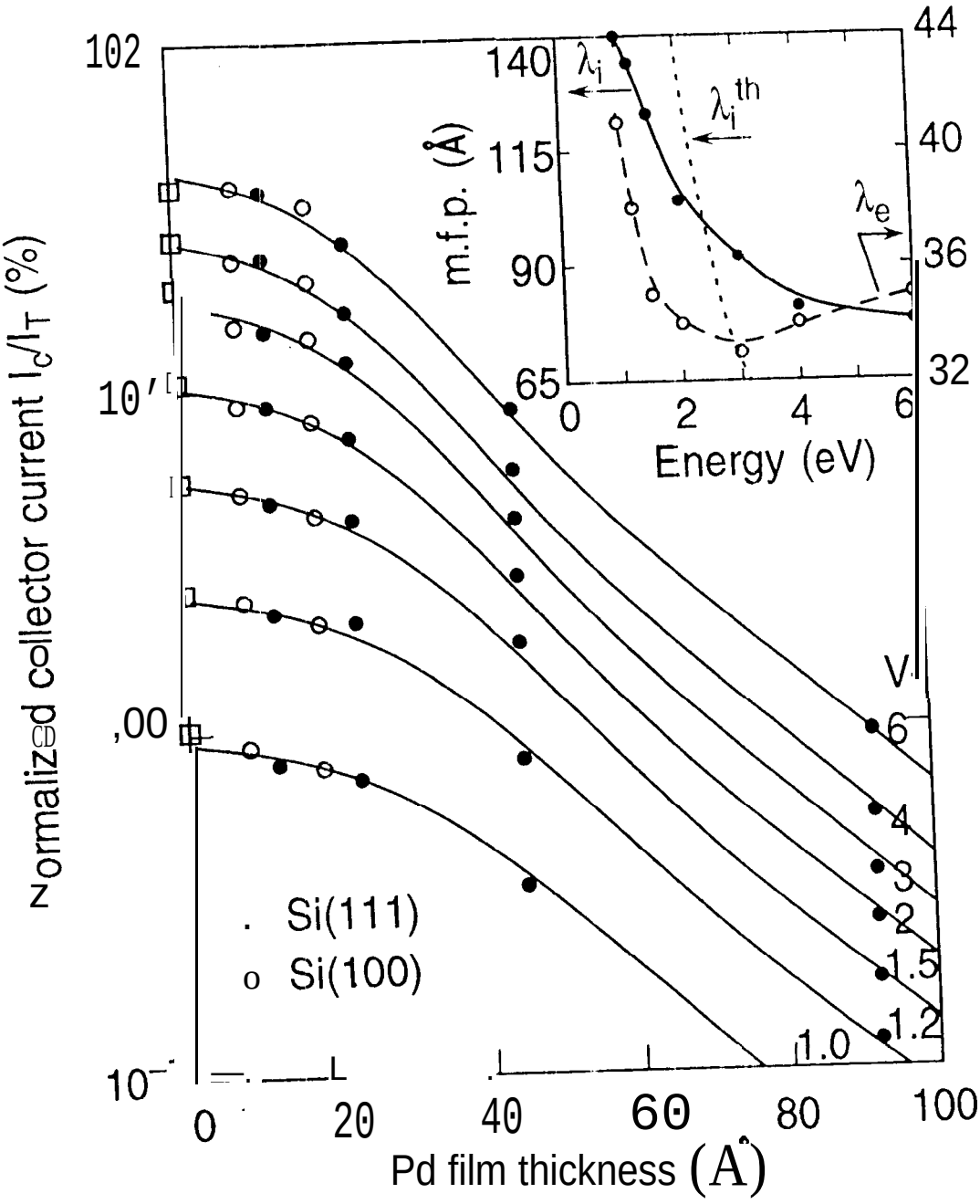

Figure 8
Bell and Kaiser
Ann. Rev. Mater. Sci.
Page 28

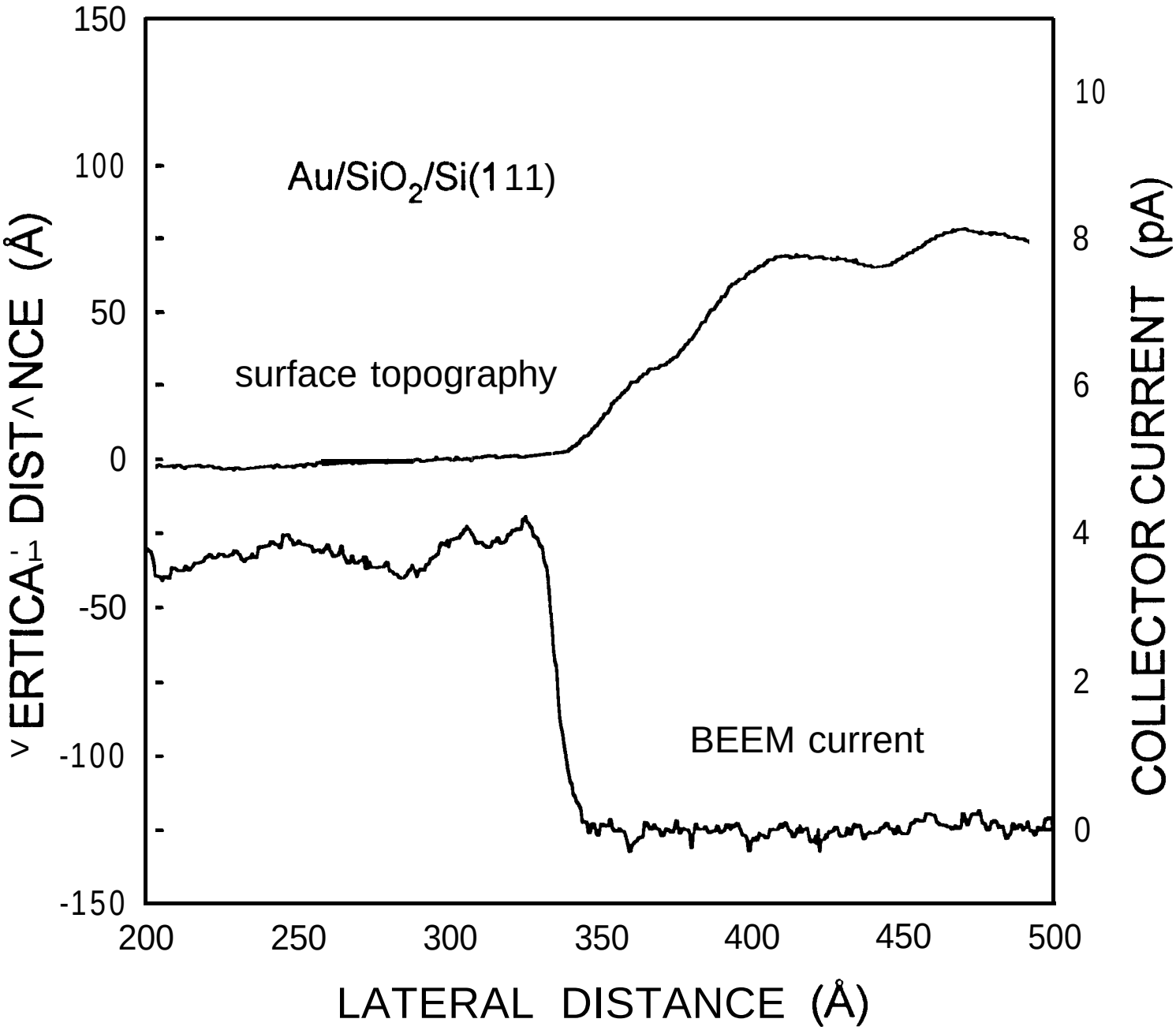

Figure 9
Bell and Kaiser
Ann. Rev. Mater. Sci.

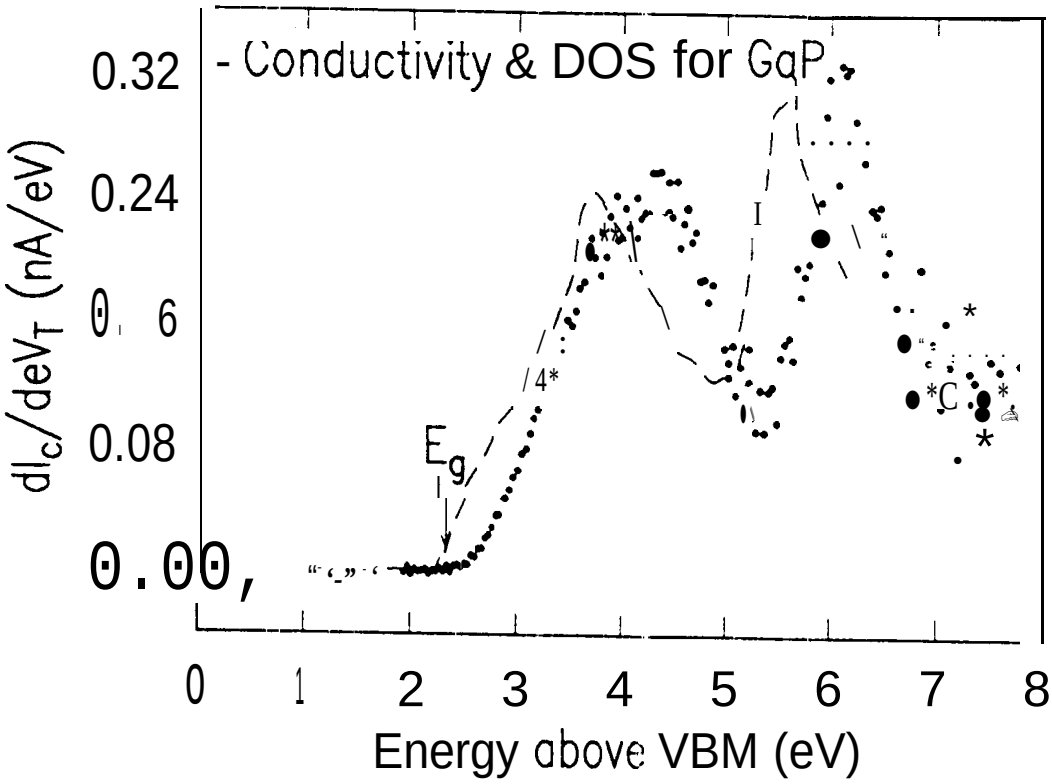

Figure 10
Bell and Kaiser
Ann. Rev. Mater. Sci.
Page 30

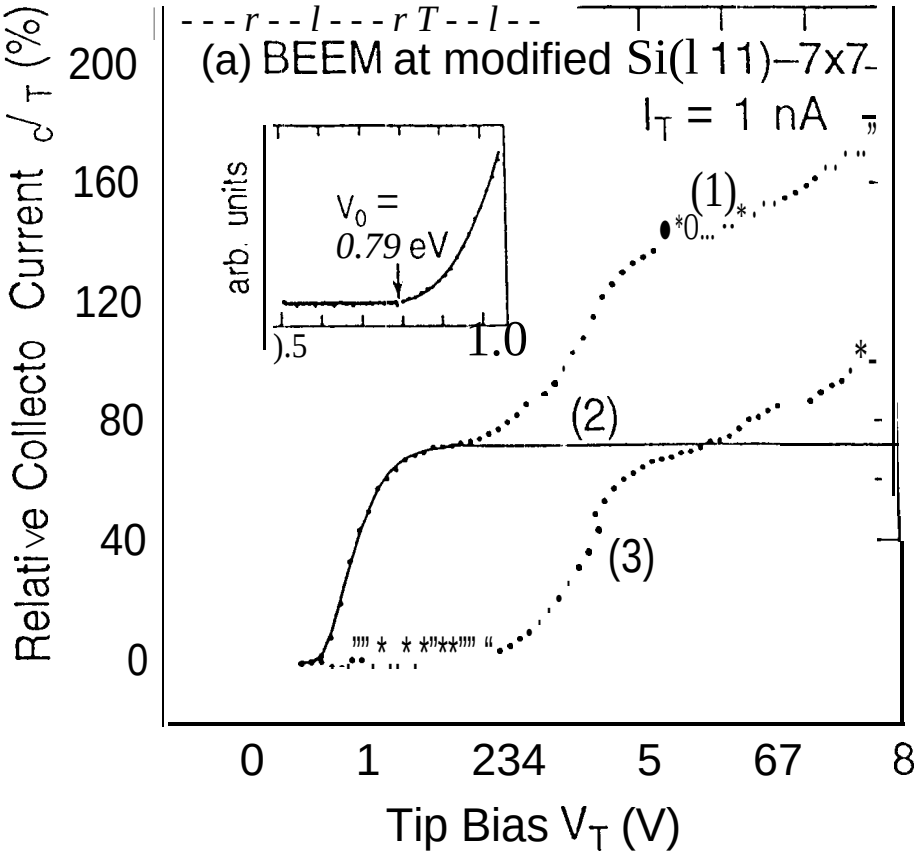

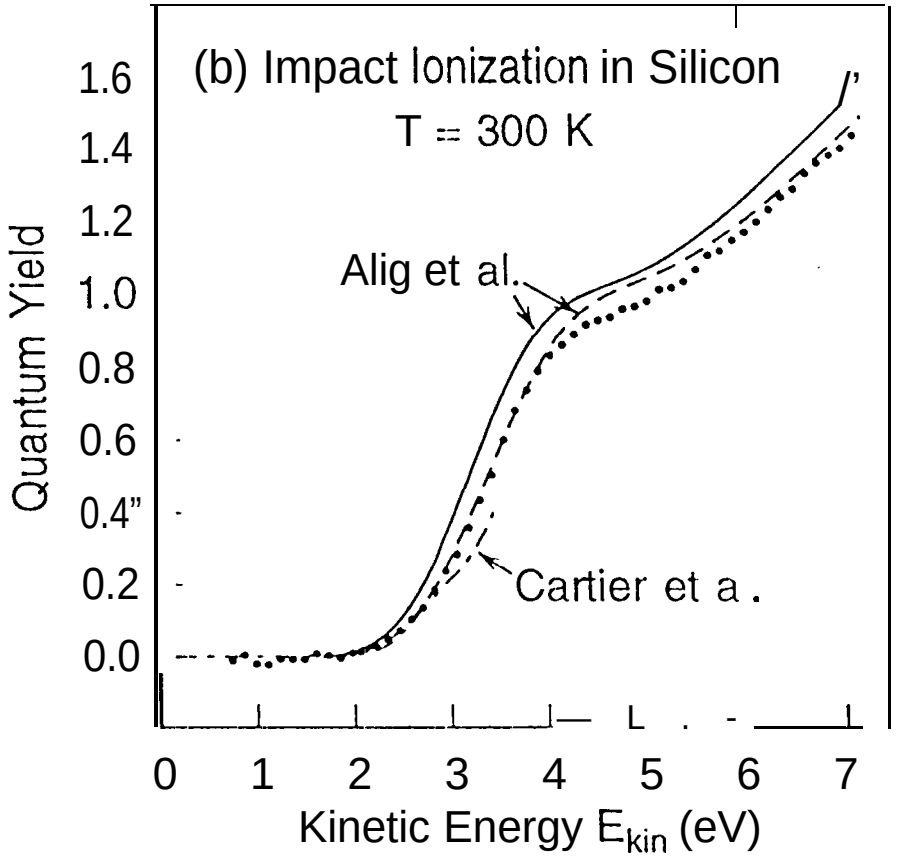

Figure 11
Bell and Kaiser
Ann. Rev. Mater. Sci.

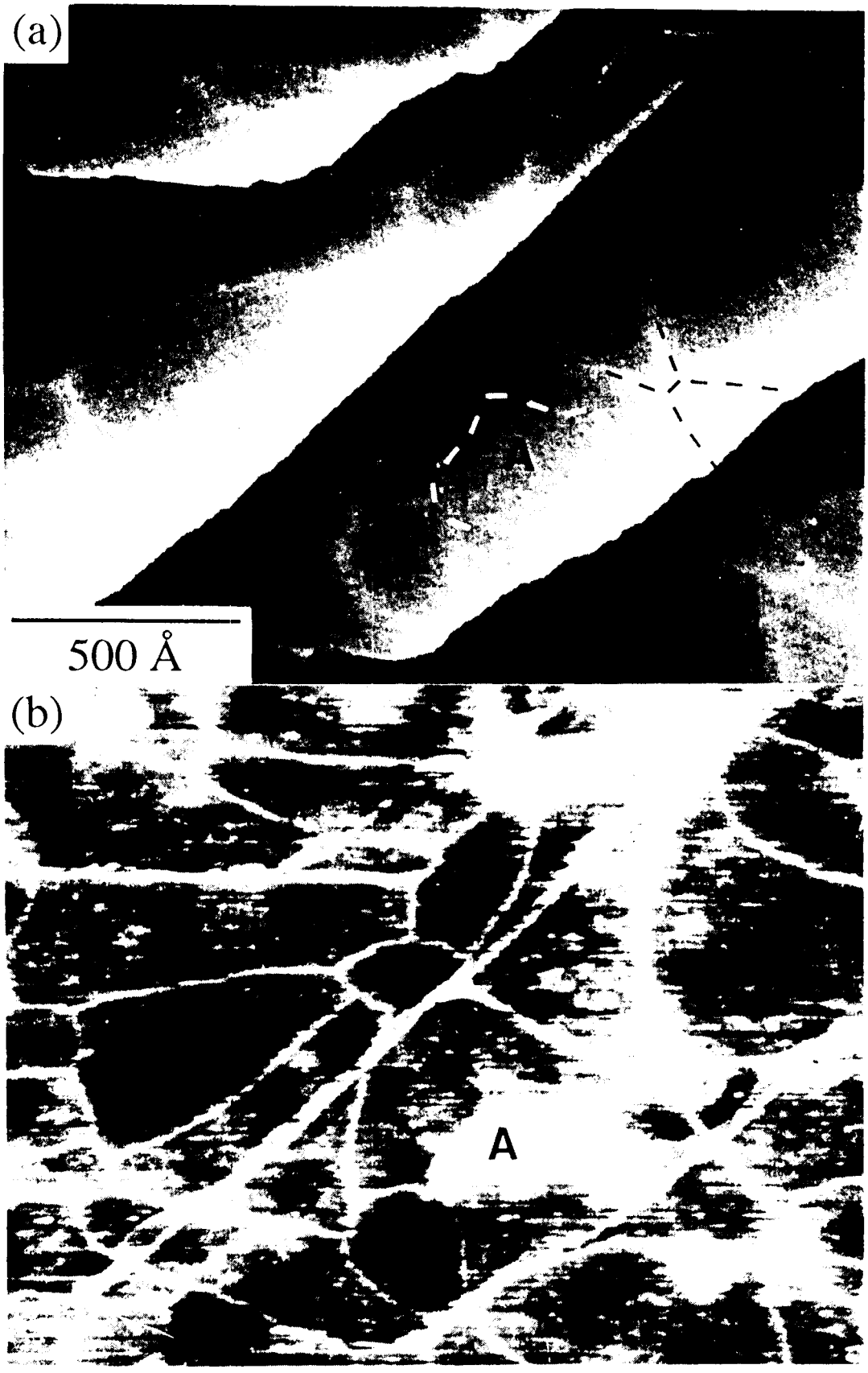

Figure 12
Bell and Kaiser
Ann. Rev. Mater. Sci.
Page ??

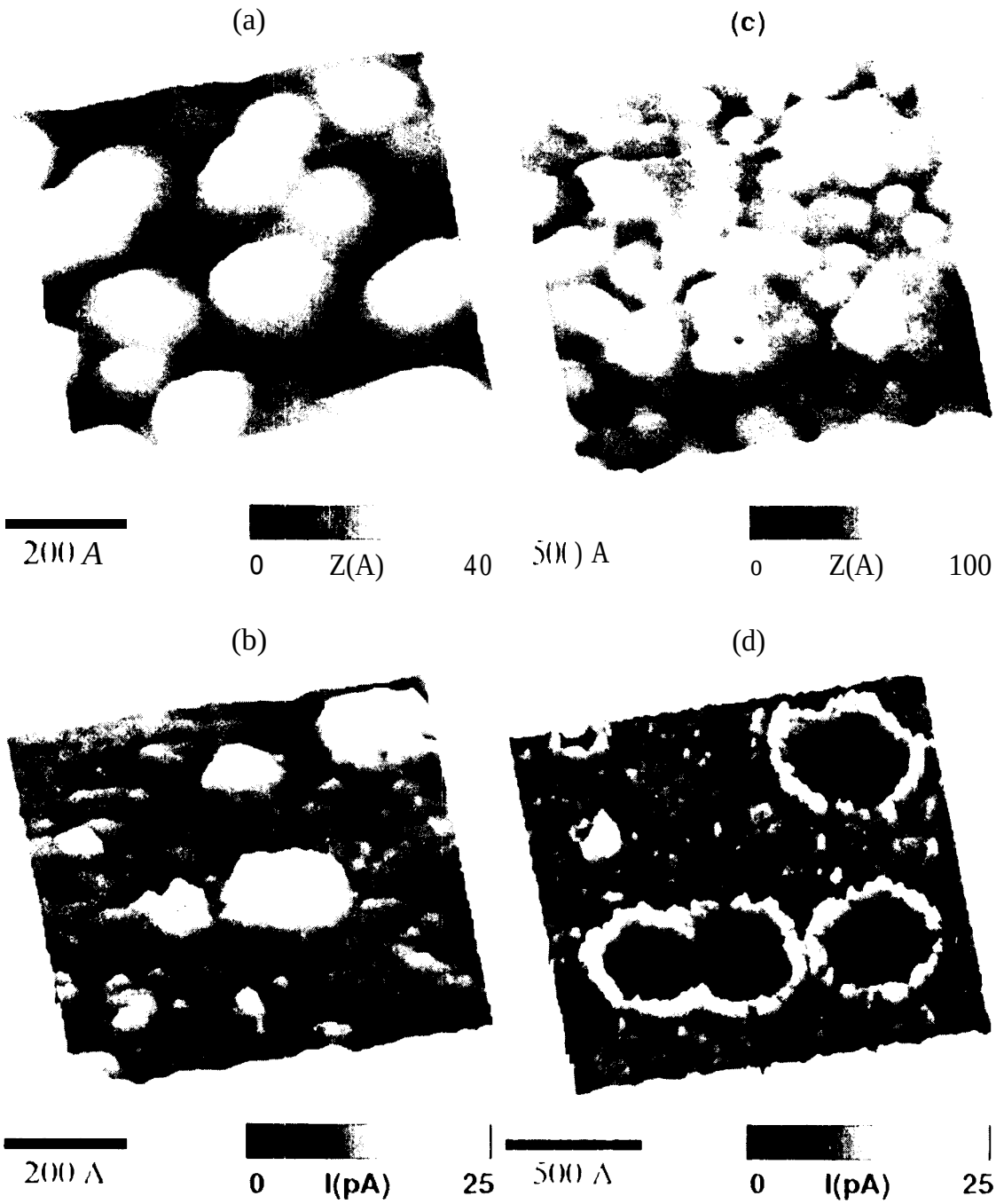

Figure 13
Bell and Kaiser
Ann. Rev. Mater, Sci.
Page 33

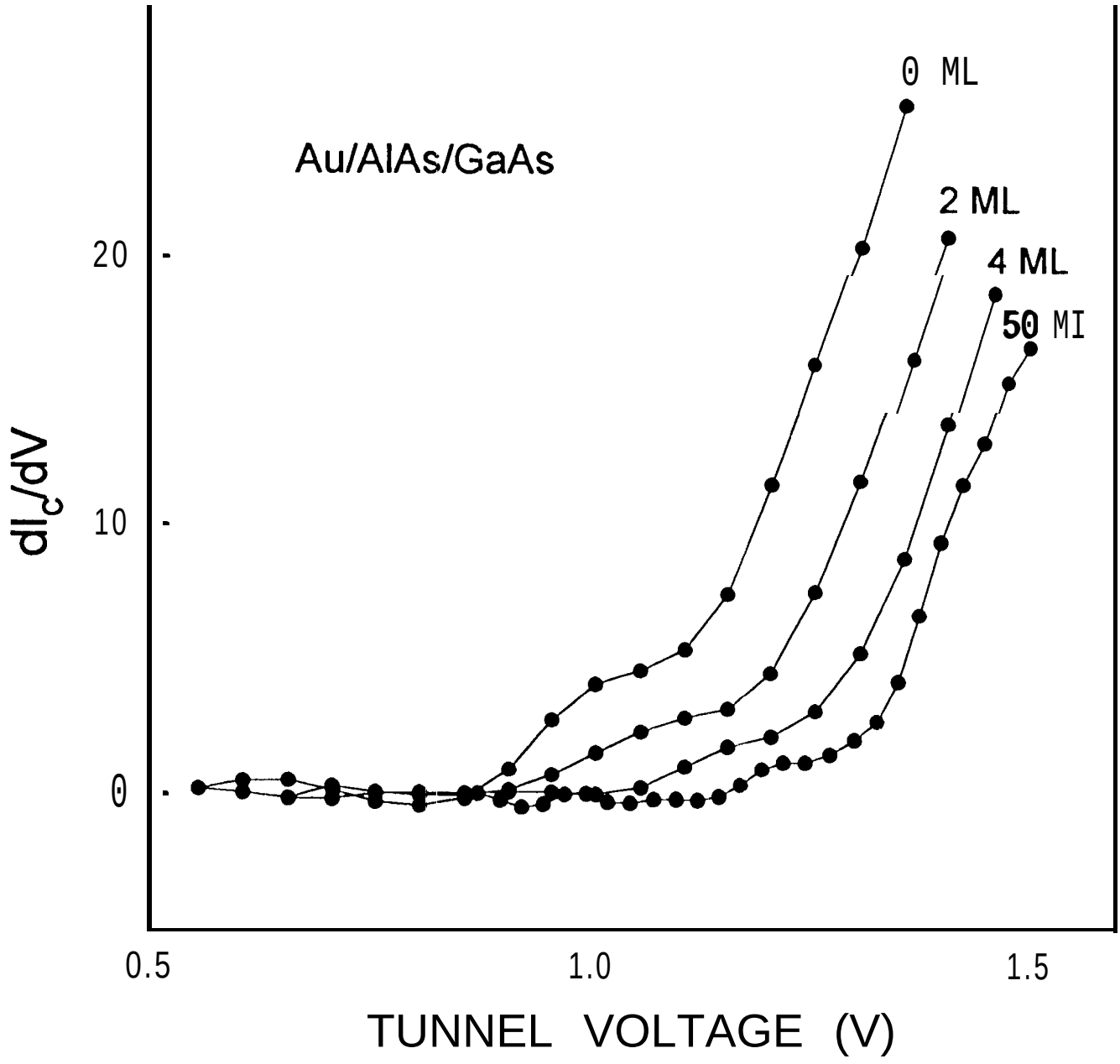

Figure 14
Bell and Kaiser
Ann. Rev. Mater. Sci.
Page 34

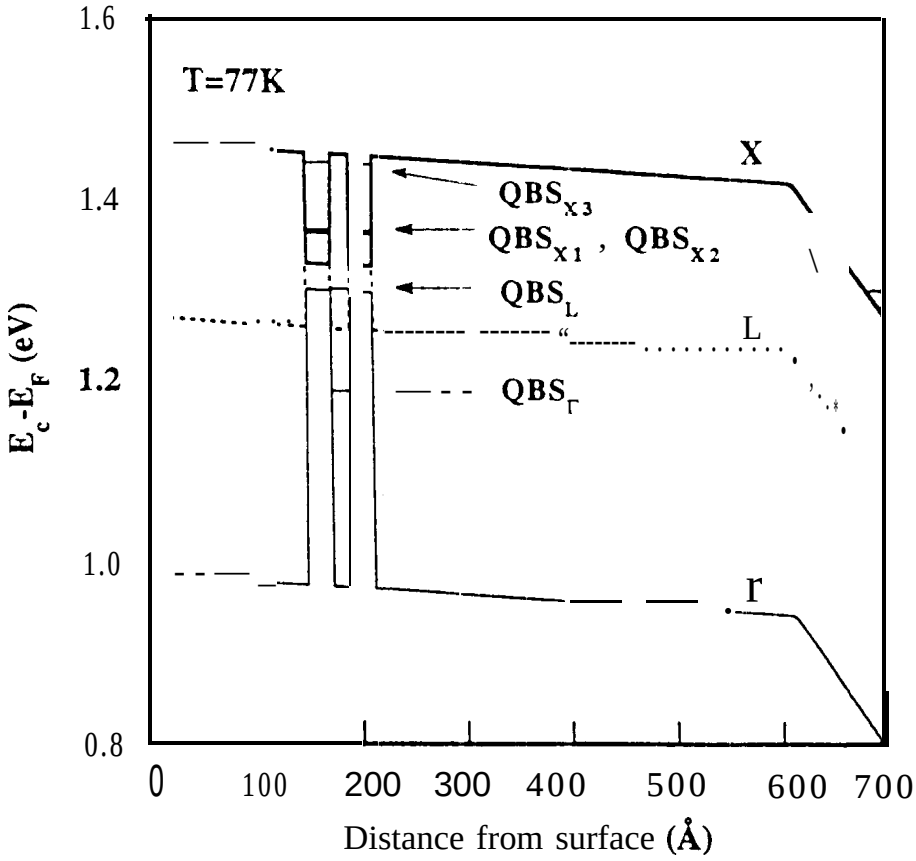

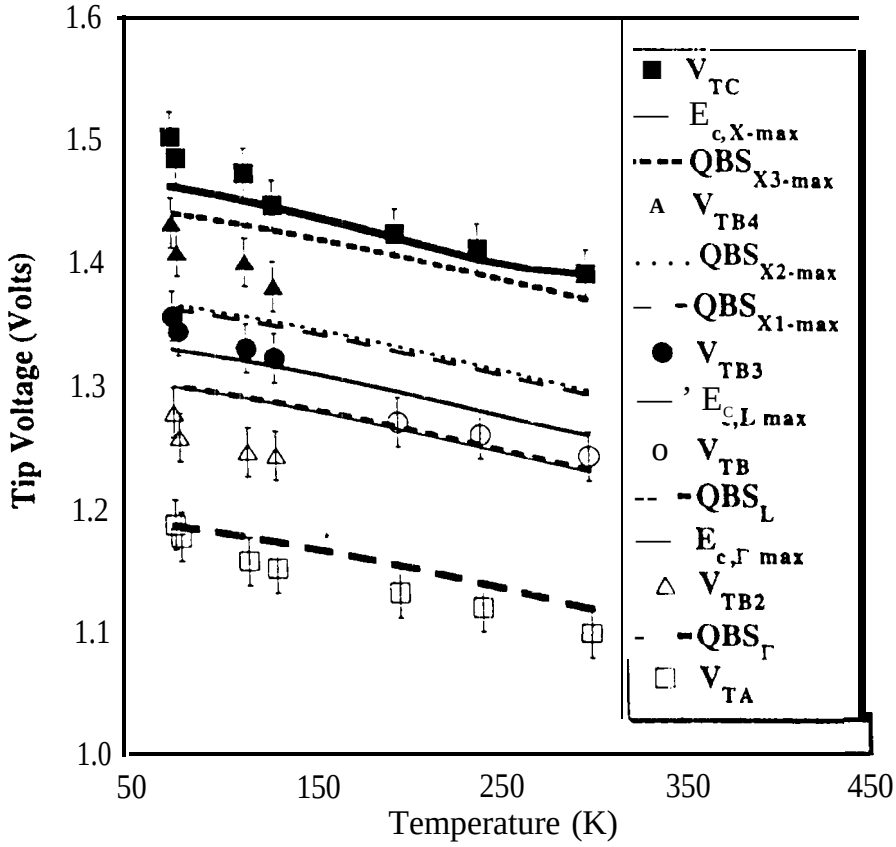

Figure 15
Bell and Kaiser
Ann. Rev. Mater. Sci.

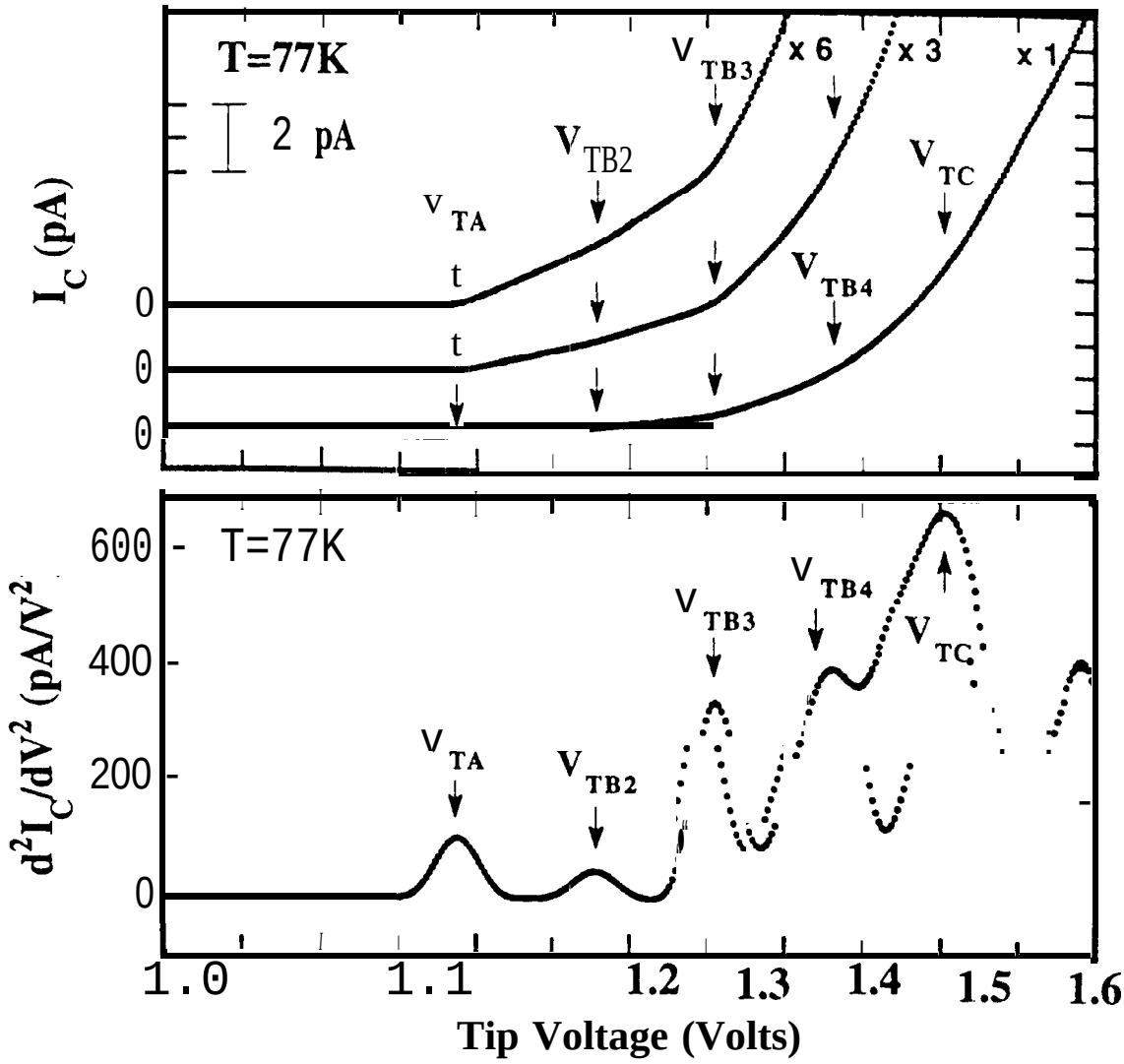

Figure 16
Bell and Kaiser
Ann. Rev, Mater. Sci.
Page 36

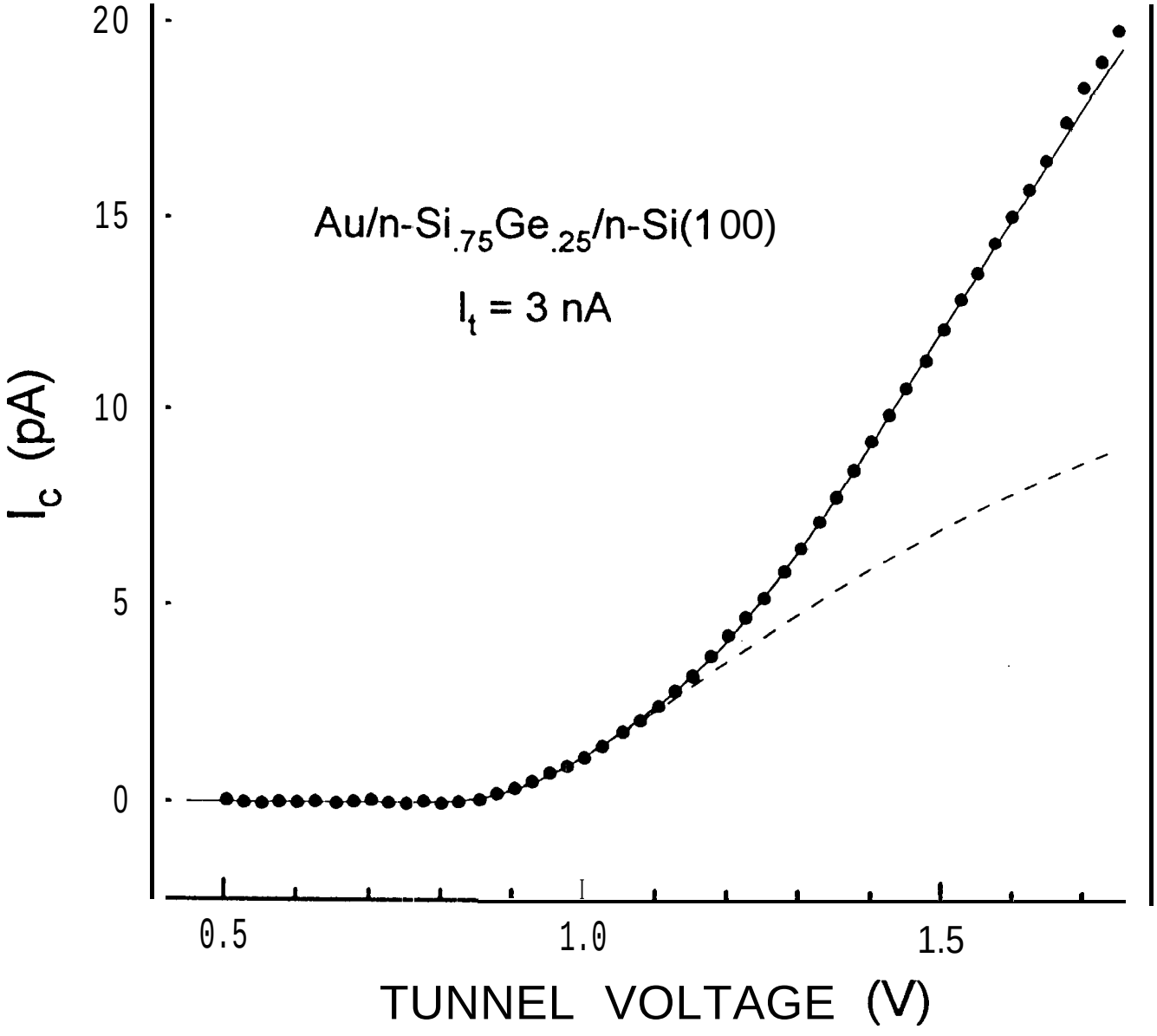

Figure 17
Bell and Kaiser
Ann. Rev. Mater. Sci.
Page 37

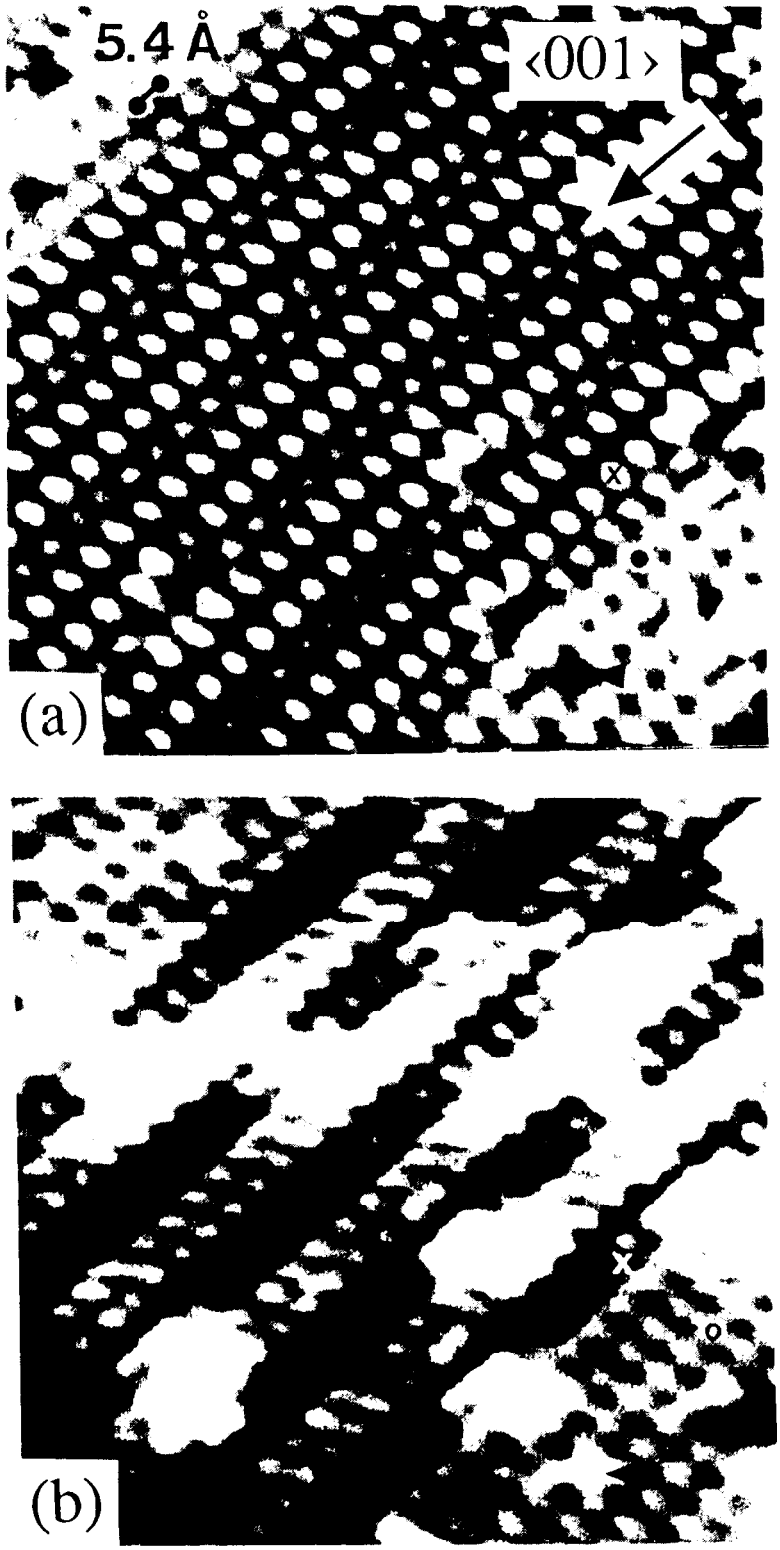

Figure 18
Bell and Kaiser
Arm. Rev. Mater. Sci.
Page 38

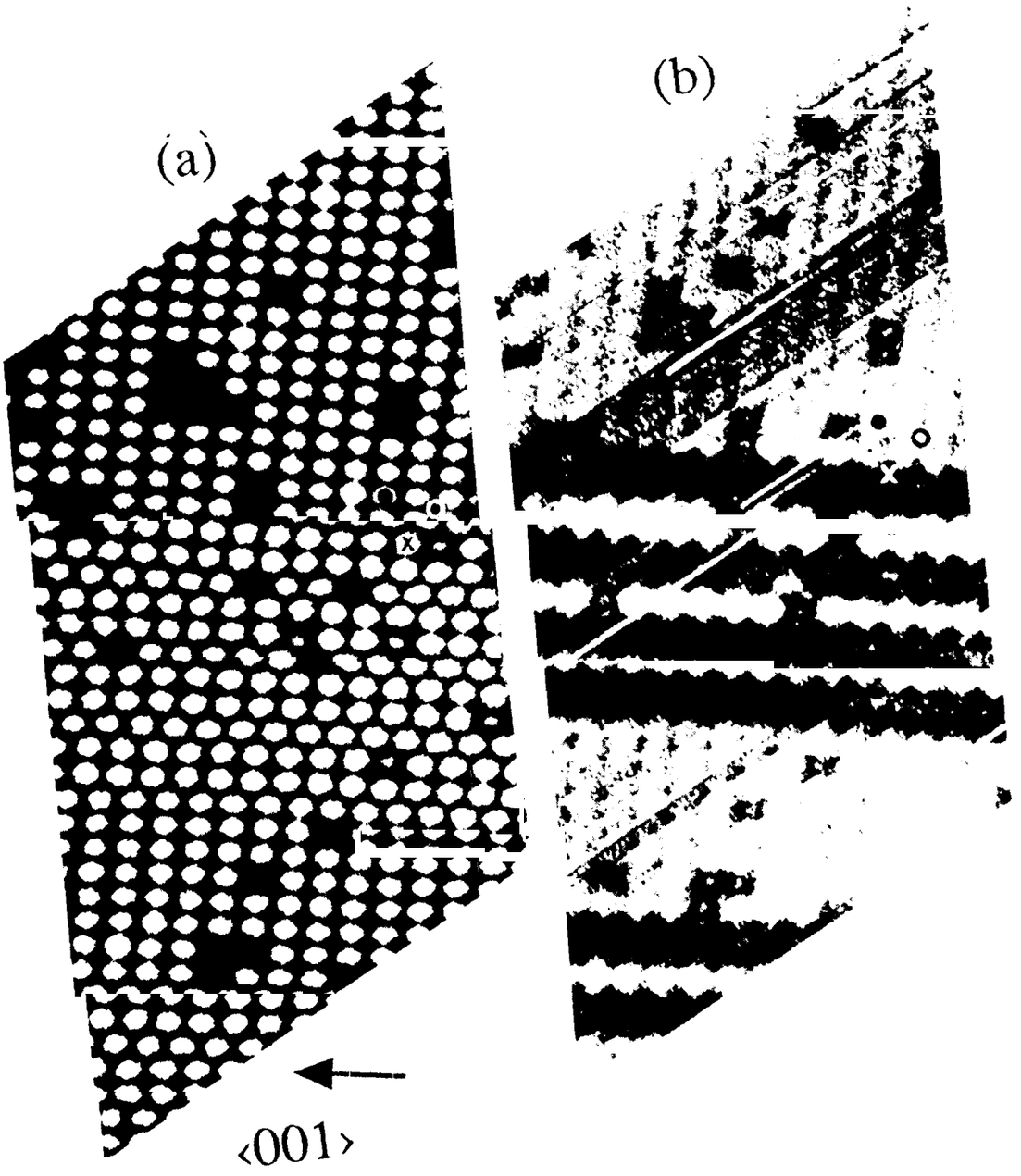

Figure 19
Bell and Kaiser
Ann, Rev. Mater. Sci.

Figure Legends

Figure 1 Energy diagram for BEEM of a metal base/semiconductor collector Schottky barrier system, for (a) applied tunnel voltage of zero, and (b) applied tunnel voltage V in excess of the interface barrier height V_b. For $V > V_b$, some of the injected electrons have sufficient energy to enter the semiconductor. Adapted from [7].

Figure 2 BEEM I_c-V spectra (dots) for (a) 8 nm Mg, (b) 20 nm Ag, (c)6 nm Au, (d) 15 nm Cu, and (e) 5 nm Ni. Arrows mark the thresholds obtained from fitting to the phase-space model with QMR included, From [22].

Figure 3 Reverse-bias dependence of the mean barrier heights determined from fitting to a phase space + QMR model. The solid curve is the expected barrier height dependence due to the image potential lowering, plotted with arbitrary offset. From [37],

Figure 4 Experimental BEEM spectrum (open circles) for Au/Si(1 11) plotted with theoretical spectra for different models. The original phase-space model is shown by triangles, and crosses represent Monte Carlo calculations which include elastic scattering. Adapted from [38].

Figure 5 BEEM spectrum of $CoSi_2$(10 nm)/n-Si(1 11). The threshold position is at about 0.85 eV, almost 0.2 eV higher than the SBH for this interface as determined by photoresponse. Adapted from [54].

Figure 6 Phase space for electron transmission through a $CoSi_2$/Si(1 11) interface. The panels show the irreducible wedge of the interface Brillouin zone of both the $CoSi_2$ and the Si. At each parallel wave vector used in the calculation there is an open circle if there is at least one state at that energy in the $CoSi_2$ and a plus if there is at least one state in the Si. If there is a state in both there is a closed circle. From [55].

Figure 7 Plot of BEEM transmittance (I_c/I_t x 100), measured at 77K (circles) and room temperature (squares) at V_t = -1.2 V. Lines represent least-squares fits to the data. The attenuation length in the Au is obtained from the slope of the lines, and the intercept yields the zero-thickness transmittance. From [64].

Figure 8 Attenuation of I_c with Pd thickness for indicated tip biases. The solid lines are fits to the data, with the mean-free paths thus obtained plotted in the inset. From [67].

Figure 9 Topographic and BEEM line scans taken from images of a $Au/SiO_2/Si(111)$ structure. Adapted from [41].

Figure 10 dI_c/dV (dots) compared with empirical pseudopotential density-of-states (dashed line) by Chelikowsky and coworkers.[77] From [75].

Figure 11 (a) Representative BEEM spectrum (curve 1) taken in a pinhole of a 2.2 nm thick B-type $NiSi_2$ film. The spectrum is decomposed into a primary electron part (curve 2) and a secondary electron part resulting from impact ionization (curve 3). The inset shows the threshold region of a similar spectrum. (b) Quantum yield (dots) as a function of kinetic energy in Si, calculated by dividing curve 3 by curve 2. The three lines represent results of theoretical calculations. From [78].

Figure 12 STM topograph (a) and corresponding BEEM image (b) obtained on a 2.5 nm $CoSi_2$/Si(111) sample (V_t = -2V, I_t = 5 nA). The dislocation network is indicated by dashed lines. Region "A" and small stripes parallel to the surface steps exhibit a 2x1 surface reconstruction. In the BEEM image brighter areas indicate regions of higher BEEM current. The arrow indicates an atomic-scale surface point defect (not resolved in the tomograph). The typical current variation on the terraces (black to white) is of the order of 50 pA for an average BEEM current of 200 pA. From [56].

Figure 13 (a) Grey-scale STM topograph and (b) BEEM image of a Au/Si sample illustrating enhancement-type modifications. The STM topograph did not visibly change as a result of the modification. All the white areas in the BEEM images were created by stressing with the STM tip. Stressing voltage ranged from 1.9 V to 2.3 V. (c) Grey-scale STM topograph and (d) BEEM image of a Au/Si sample illustrating a reduction-type modification, Four major areas of BEEM reduction are seen, with corresponding modifications of surface topography. Adapted from [61].

Figure 14 Derivatives dI_c/dV for BEEM spectra of Au/AlAs/GaAs structures. Data are shown for AlAs thicknesses of 2 ML, 4 ML, and 50 ML. Also shown is a derivative spectrum for Au/GaAs (labeled "O ML"). Adapted from [105].

Figure 15 (a) DBRTS band profiles and quasi-bound states for the Γ, L, and X bands at 77K. (b) T dependence of the calculated energy levels and the measured thresholds deduced from Figure 17. Solid lines correspond to the band edges, and dashed or dotted lines represent quasi-bound states. From [87].

Figure 6 I_c-V and d^2I_c/dV^2-V for the DBRTS at 77K From [87].

Figure 17 BEEM I_c-V spectrum for a Au/$Si_{.75}Ge_{.25}$/Si(100) heterostructure. The data are shown by circles. Also plotted are two theoretical spectra which have been fit to the data. The first (dashed line) fits only the low-voltage portion (V < 1.1 V) with a single threshold; the other fit (solid line) is over a larger range (to 1.6V) using a Iwo-threshold model. The extracted thresholds for the two-threshold fit are separated by 304 mV. Adapted from [97].

Figure 18 STM topograph (a) and simultaneously recorded BEEM image (b) on the Si-rich $CoSi_2$/n-Si(100) surface (V_t = -1. 5V, I_t = 3 nA, film thickness = 3.8 rim). The center part displays a $3\sqrt{2} \times \sqrt{2}R45°$ reconstruction, whereas the lower right is $\sqrt{2} \times \sqrt{2}R45°$ reconstructed. The $\sqrt{2}$ topographic corrugation is 0.015 nm. The displayed BEEM range is from 25 pA (black) to 55 pA (white). From [112].

Figure 19 STM topograph (a) and reverse BEEM image (b) on a $3\sqrt{2}/\sqrt{2}$ surface region of $CoSi_2$/n-Si(100) (V_t = 2V, I_t = 10 nA, film thickness= 3.8 rim). The displayed BEEM range is from 5 pA (black) to 12 pA (white). From [1 12].